Sedimentology and chemostratigraphy of Carboniferous red beds in the western Moncton Basin, Sussex area, New Brunswick, Canada: possible evidence for a middle Mabou Group unconformity

M. M. Nazrul Islam and David G. Keighley*

Department of Earth Sciences, University of New Brunswick, Fredericton, New Brunswick E3B 5A3, Canada
*Corresponding author <keig@unb.ca>

Date received: 30 November 2017 ¶ Date accepted: 12 July 2018

ABSTRACT

The area around Penobsquis, east of Sussex, New Brunswick, Canada, is an important location of natural resources for the province. The McCully gas field produces from strata of the Mississippian Horton Group whereas younger strata of the Windsor Group are host to major potash and rocksalt deposits. Overlying these units are over 1 km of poorly understood red beds currently assigned to the Mississippian Mabou Group. To date, this latter unit lacks significant marker beds and has had no useful biostratigraphic recovery, despite recent extraction of close to 5 km of drill core. Research on this core broadly identifies siltstone and sandstone at the base of the Mabou Group that gradually coarsen up into conglomerate. The succession is considered the result of alluvial-fan progradation from the northeast. Within this succession, in several of the cores, is a single interval of localized, horizontally laminated to cross-stratified, bluish-grey sandstone, containing carbonaceous plant fragments and siltstone intraclasts. To assess the importance of this interval in the context of the red bed succession, a total of 131 samples of core from three boreholes have been analyzed using Inductively Coupled Plasma and spectroscopic techniques to determine chemostratigraphy. Study of various elemental ratios can delineate two packages, one that corresponds to the grey interval and overlying red beds, and the other to the underlying red beds. Changes in the elemental ratios are interpreted to mark a broader population of mineral species related to greater variation of provenance and diagenesis in the upper sediment package. The reduced horizons and rip-up clasts may have been produced by sediment reworking along a boundary that represents an unconformity (in core, a disconformity) at a stratigraphic level near to where one has been inferred by other workers.

RÉSUMÉ

La région entourant Penobsquis, à l'est de Sussex, au Nouveau-Brunswick, au Canada, est un lieu important sur le plan des ressources naturelles pour la province. Le champ de gaz naturel McCully tire ses ressources des strates du groupe de Horton, dans le Mississippien, tandis que les strates plus récentes du groupe de Windsor recèlent d'importants gisements de potasse et d'halite. Plus d'un kilomètre de couches rouges mal comprises, actuellement attribuées au groupe de Mabou, dans le Mississippien, recouvre ce champ. À ce jour, ces couches sont exemptes d'horizon repéré significatif et n'ont fait l'objet d'aucune récupération biostratigraphique utile malgré l'extraction récente de carottes de forage totalisant près de 5 km. Selon les recherches menées sur ces carottes, on y retrouve à la base du groupe de Mabou de grandes quantités de stiltite et de grès qui se transforment graduellement en conglomérat. Cette succession est considérée comme le résultat de la progradation d'un cône alluvial provenant du nord-est. On y a également découvert dans plusieurs carottes un intervalle localisé de grès bleu-gris à lamination horizontale à croisée, contenant des fragments de plantes carbonées et des intraclastes de stiltite. Pour évaluer l'importance de cet intervalle dans le contexte de la succession de couches rouges, 131 échantillons de carottes au total tirés de trois trous de forage ont été analysés au moyen des techniques spectroscopiques et de plasma à couplage inductif afin de déterminer la chimiostratigraphie. L'étude de divers ratios élémentaires permet de circonscrire deux ensembles, un correspondant à l'intervalle gris et aux couches rouges supérieures, l'autre correspondant aux couches rouges inférieures. L'interprétation des différences dans les ratios élémentaires permet ensuite de repérer une population plus marquée d'espèces minérales en lien avec une diversité accrue de provenances et une diagénèse dans l'ensemble de sédiments supérieur. Les horizons réduits et les clastes arrachés pourraient être issus du remaniement des sédiments le long d'une frontière constituant une discordance (une discordance stratigraphique dans la carotte) à un niveau stratigraphique près de l'endroit où d'autres travailleurs ont inféré pareille discordance.

[*Traduit par la redaction*]

ATLANTIC GEOLOGY 54, 285–314 (2018)
0843-5561|18|0285–0314$5.50|0
doi:10.4138/atlgeol.2018.010

INTRODUCTION

Chemostratigraphic methods include those that characterize sedimentary successions based on distinctive features in their inorganic whole-rock geochemistry. Their applications have most commonly been in the subdivision of deformed red beds, where biostratigraphic and magnetostratigraphic methods are limited by lack of preserved microfossils and uncertain reorientation of magnetic minerals in the strata (e.g., Preston *et al.* 1998; Pearce *et al.* 1999, 2005, 2008; Ratcliffe *et al.* 2004, 2010).

Red beds are common in Upper Devonian to Pennsylvanian strata of southeastern New Brunswick, where they form part of the fill in a system of basins (Cocagne Graben, Moncton, Sackville, and Cumberland basins) that are components of the regional Maritimes Basin Complex (Fig. 1; Keighley 2008). Three tectono-sedimentary megacycles ("allocycles" of St. Peter 1993) have been identified (Fig. 2) that indicate a complex history of fault-controlled subsidence, strike-slip motion, basin inversion, and salt tectonics (e.g., Wilson 2005; Wilson and White 2006; Park and St. Peter 2009; Park *et al.* 2007, 2010; Waldron *et al.* 2013; Craggs *et al.* 2017). Red beds are particularly abundant in the 2nd megacycle (Upper Mississippian), where they have been formally differentiated into several formations in the Moncton and adjacent basins. However, in the western part of the Moncton Basin, limited outcrop and borehole data to date have resulted only in a few broadly based studies of the Upper Mississippian red beds (Anderle *et al.* 1979; Wilson 2005), an informal lithostratigraphy at the sub-group level (St. Peter 1993), and continued uncertainty as to the presence or importance of a mid-red bed unconformity first inferred by Gussow (1953) and subsequently by Jutras *et al.* (2007) farther north in southern Québec and northern-most New Brunswick. Limited spore recovery from these red beds also has hindered biostratigraphic subdivision (St. Peter and Johnson 2009).

A recent potash exploration program by the Potash Corporation of Saskatchewan Inc. (PotashCorp), near Sussex, now has resulted in the collection of over 5 km of drill-core. Sedimentary logging of these cores, together with bulk-rock Inductively Coupled Plasma – Mass Spectrometry (ICP-MS) analyses of 131 samples from three of the cores, allows for new insights into the red bed succession, the informal stratigraphy, and supporting evidence for the previously identified unconformity. The results further confirm the utility of whole-rock chemostratigraphy.

GEOLOGICAL SETTING

The > 3.5 km-thick Devonian-Carboniferous stratigraphic succession in southern New Brunswick overlies terranes (southwards, Ganderia, Avalonia, and, in Nova Scotia, Meguma) that accreted to Laurentia in the Silurian-Devonian (Fig. 1). However, in this region these terranes were still subject to later relative movements accompanying oblique collision of Gondwana to Laurentia (Alleghanian orogeny, Murphy *et al.* 2011; Waldron *et al.* 2015). This provided a major transtensional-transpressional structural control on the younger stratigraphy. Initially, the result was the development of small-scale sedimentary pull-apart basins, such as the Moncton Basin (Craggs *et al.* 2017).

The three tectono-sedimentary megacycles recognised in the New Brunswick Devonian-Carboniferous succession (Fig. 2; St. Peter 1993) are separated by interbasinal angular unconformities related to specific tectonic episodes (Murphy *et al.* 2011). More localized intrabasinal unconformities are identified within individual basins. The first megacycle, which culminated in a late Tournaisian to early Visean inversion, consists of strata assigned to the Horton and Sussex groups. The second megacycle contains strata assigned to the Windsor and Mabou groups. The subsequent late Visean to Serpukhovian inversion (Wilson and White 2006; Murphy *et al.* 2011), is related to the near-continent-wide Mississippian-Pennsylvanian unconformity, and in eastern Canada is signified by a major episode of transpression and uplift associated with the Minas Fault Zone (Fig. 1a; Murphy *et al.* 2011). Early Pennsylvanian deposition (Cumberland Group) again appears to have been initiated in areas of transtension, and rapidly subject to salt tectonism associated with deformation of buried Windsor Group evaporites (Waldron *et al.* 2013; Craggs *et al.* 2017). However, in the later Pennsylvanian, thermal relaxation caused regional cooling and subsidence, leading to the development of an enlarged sedimentary basin, which buried most of the rapidly deposited, locally sediment-sourced, and deformed pull-apart basins. Therefore, in contrast to the first two megacycles, the third evolved to also consist of a blanket of more mature, generally more slowly accumulated sediment (Pictou Group) in a more regional terrestrial drainage sys-tem (Gibling *et al.* 1992).

The focus of this paper is on red beds currently included in the upper Mississippian 2nd megacycle (Fig. 2). Within this megacycle, carbonate and evaporite rocks are interpreted to have been deposited following marine transgressions, and red beds to have followed regional uplift or marine regression (Giles 1981, 2009; Wilson 2005). Various formations are combined into the Windsor Group, the lower and upper

Figure 1. (next page) (a) General geological map of eastern Canada showing the main basement terranes and erosional remnant of the Maritimes Basin Complex (after Craggs et al, 2017). (b) Geological map of southern New Brunswick detailing the occurrence of Carboniferous strata in the Moncton Basin (after Craggs *et al.* 2017). (c) Map of the area east of Sussex, New Brunswick. The old mine extracted salt and potash from the northern limb of a subsurface salt diapir. Almost all gas production from the McCully field has been from beneath this limb. New salt exploration boreholes (colour coded) are located south of the diapiric axis.

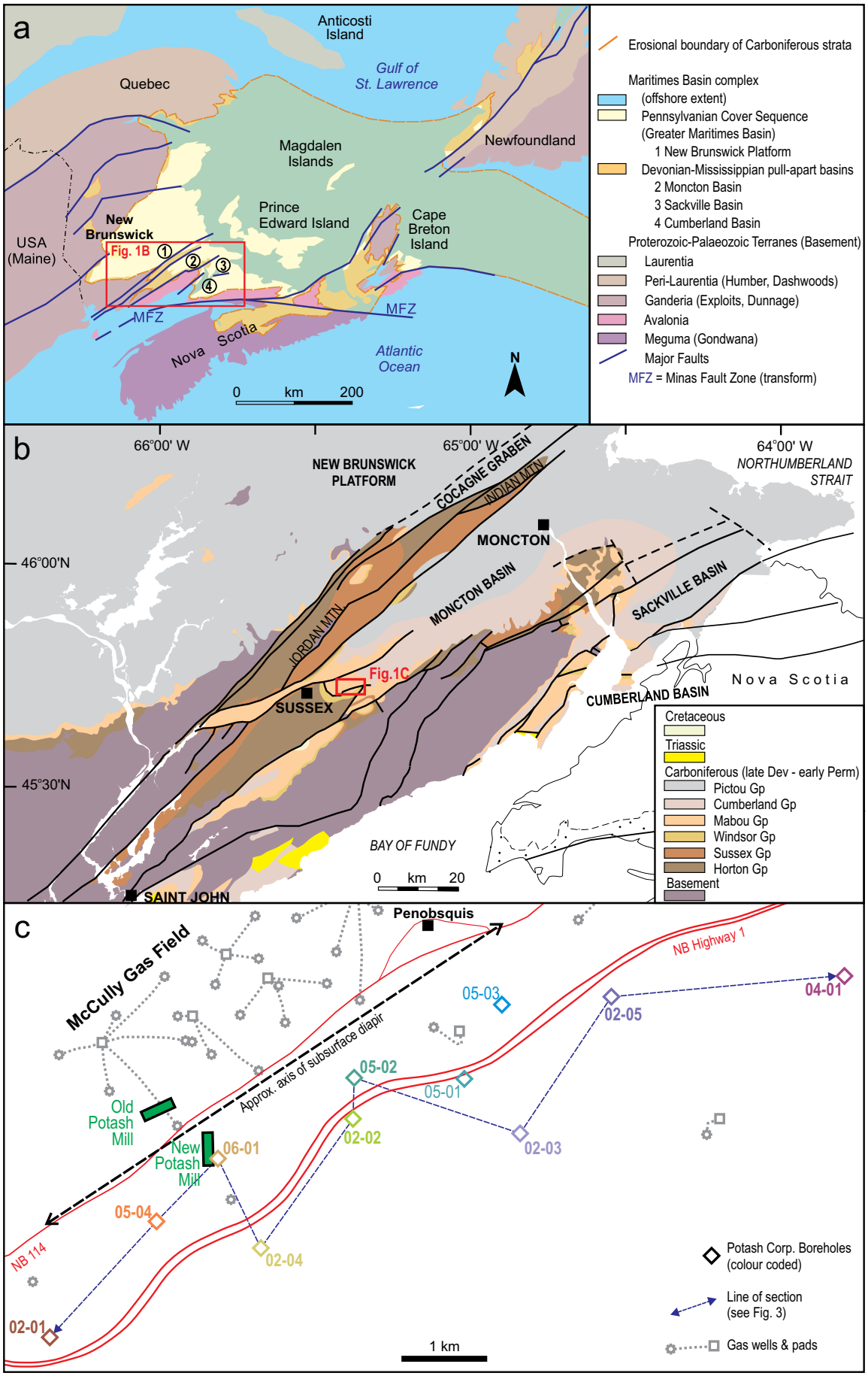

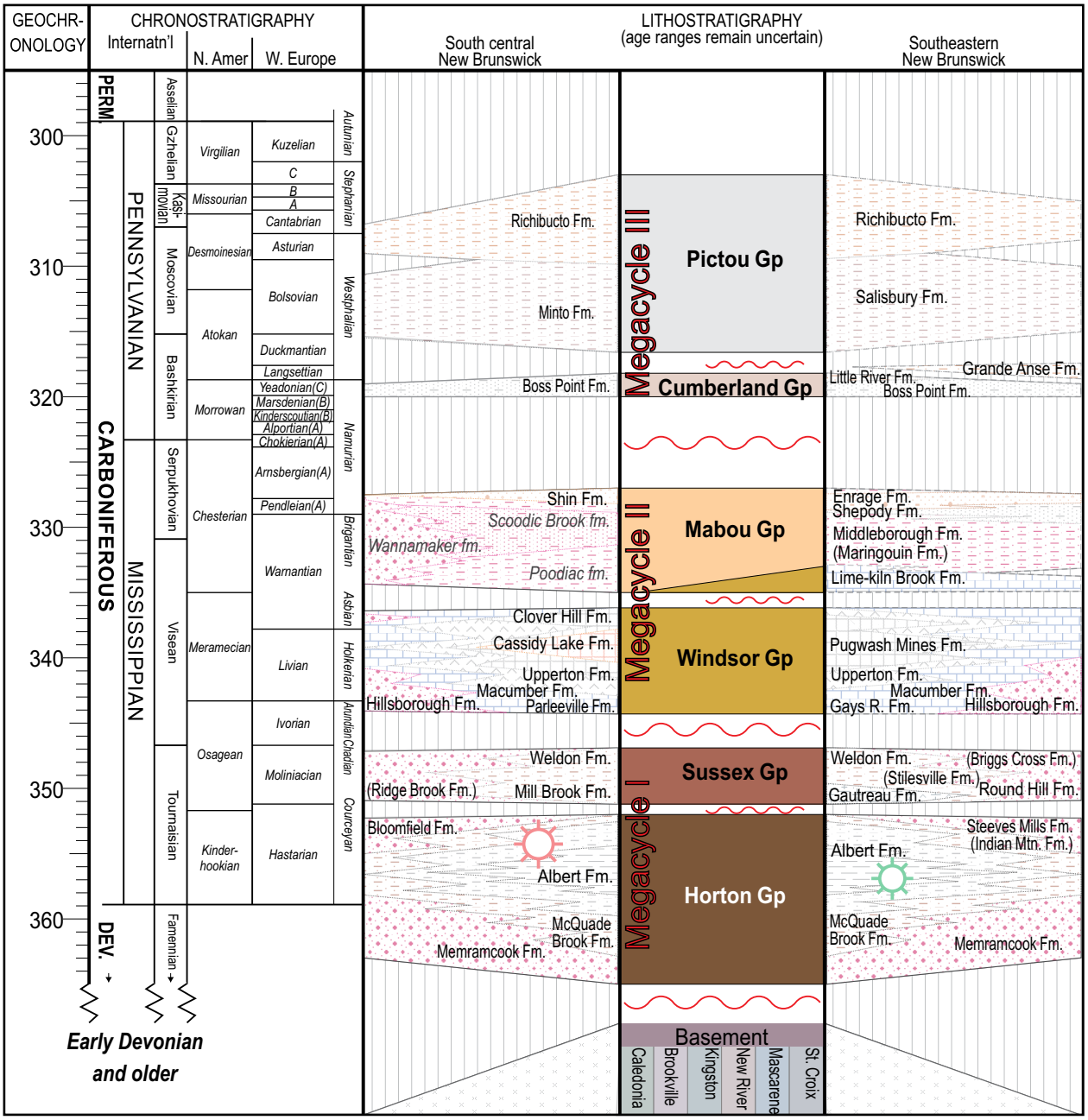

Figure 2. Stratigraphic subdivisions of southern New Brunswick including the Moncton Basin (after Keighley 2008; Craggs *et al.* 2017). Oil (green well symbol) and gas (red well symbol) are extracted from the Albert Formation.

contacts of which are placed at the base and top of the stratigraphically lowest and highest carbonate or evaporite beds encountered in a particular area (Giles 1981; McCutcheon 1981). In the western Moncton Basin, the uppermost Windsor Group comprises the mined potash and halite (Cassidy Lake Formation) and overlying anhydrite and halite (Clover Hill Formation, McCutcheon 1981; Wilson *et al.* 2006).

In Nova Scotia, additional cycles of red beds, carbonate rocks, and sulfate rocks are reported overlying Cassidy Lake equivalent strata (e.g., Giles 2009); in New Brunswick a red bed succession up to 1 km thick overlies the Cassidy Lake Formation (Webb 2009). Originally considered part of the Gypsiferous Formation (Lyell 1843) or part of Division 8 of the Coal Measures (Logan 1845), and later the Bonaventure Formation (Logan 1864), these red beds in the far southeast of New Brunswick were formally assigned to the Hopewell Group and divided into three units by Norman (1941a, b) and Gussow (1953). A lower, red mudstone-dominated unit (Maringouin Formation, now Middleborough Formation, Jutras *et al.* 2016), is overlain by interbedded red and grey sandstone, red and grey mudstone, and minor calcareous mudstone-pebble and coalified plant-fragment conglomerate, with Cu-mineralized horizons at the base of the unit (Shepody Formation). The uppermost red beds are inter-

bedded conglomerate, sandstone, and mudstone (Enragé Formation). Toward the basin margins, a localized conglomeratic unit interfingers with and progressively overlies Windsor Group strata (Hopewell Cape Formation). Despite the ear-lier names noted above, for stability of nomenclature most authors (e.g., Wilson *et al.* 2006; Force and Barr 2006; St. Pe-ter and Johnson 2009; Utting *et al.* 2010; Murphy *et al.* 2011; Allen *et al.* 2013; Waldron *et al.* 2013; Hayward *et al.* 2014; Holt *et al.* 2014; Stimson *et al.* 2016; Craggs *et al.* 2017) in-clude these and laterally equivalent red bed units sitting on Windsor Group strata in the Mabou Group of Belt (1964, 1965). Overlying plant-bearing grey sandstone, mudstone, and thin coal beds are assigned to the Boss Point Formation (Cumberland Group, Pennsylvanian).

In the Sussex region, the informal units of Anderle *et al.* (1979) have been used for the post-Windsor red beds, namely: grey and reddish brown sandstone, siltstone, and minor conglomerate for the Poodiac formation; greyish red conglomerate, and minor sandstone and siltstone for the Wanamaker formation; and red siltstone, and fine sandstone for the Scoodic Brook formation (note that, following the North American Commission on Stratigraphic Nomenclature, 1983, informal names do not warrant capitalization of "formation").

There has been much debate regarding the nature of the contacts associated with the post-Windsor red beds. Gussow (1953) proposed that a "mid-Hopewell" unconformity separating the Shepody and Enragé formations was equivalent to the Mississippian-Pennsylvanian boundary. As evidence, in a seismic-based cross-section (adjacent to the current study area) he interpreted Shepody-involved thrust faulting to be regionally truncated by overlying Enragé Formation. This latter formation, and its equivalent Claremont Formation in Nova Scotia, also have been assigned to the overlying (i.e., 3rd megacycle) Pennsylvanian Cumberland Group by Ryan and Boehner (1994). More recent seismic interpretations identify "a local intra-Mabou unconformity" adjacent to a thrust-related triangle zone, with Gussow's regional Mississippian-Pennsylvanian boundary unconformity picked at the Enragé – Boss Point contact (Wilson and White 2006). This latter contact for the Mississippian-Pennsylvanian boundary is also supported by the palynological work of Utting *et al.* (2010).

In Québec, Jutras *et al.* (2001) noted a channelized disconformable contact between underlying red clastic rocks of the type Bonaventure Formation and the overlying plant-bearing grey clastic rocks of the Pointe Sawyer Formation. Although lacking biostratigraphic control, the underlying red beds were considered time equivalent to the upper Windsor Group strata of Nova Scotia and named the Percé Group by Jutras and Prichonnet (2005). As noted above, this splitting of the red beds has not been adopted by other workers in New Brunswick and Nova Scotia.

METHODS

Drill cores (2.5 inch, or 63.5 mm, diameter) from the 2002, 2005, and 2006 PCS exploration program were selected. From southwest to northeast of the study area (Fig. 1c) these holes are named: PCS-02-01, PCS-05-04, PCS-02-04, PCS-06-01, PCS-02-02, PCS-05-02, PCS-02-03, PCS-02-05, and PCS-04-01. Cores from PCS-05-01 and PCS-05-03 were excluded from detailed lithofacies analysis because they are highly fractured. Logging of the approximately 4 km of core was undertaken at the centimetre scale from the depth where coring began in the red beds, down to the contact with underlying evaporite or carbonate; study of Windsor Group strata did not form part of this project. Lithofacies analysis was based on the classification scheme of Miall (1978, 1996).

A small biostratigraphic study was attempted on material from grey siltstone beds but no palynologic components were identified that could narrow down the time of deposition beyond what is already known and stated above (G. Dolby, personal communication, 2013).

Several of the logged boreholes were also selected for geochemical sampling. For PCS-02-05, 59 samples were collected systematically at regular (~10 m) intervals. For boreholes PCS-05-04 (n = 44) and PCS-02-01 (n = 30), samples were collected by random number generation (converted to borehole depth) using Microsoft Excel to achieve more unbiased results. In all cases, to minimize variation resulting simply from grain size factors (Pearce *et al.* 1999), materials were collected from the finest grained beds within 1 m of the designated sampling depth.

Following Pe-Piper *et al.* (2008), sample preparation and analyses were performed by Activation Laboratories Ltd. (Actlabs) in accordance with the International Organization for Standardization (ISO) 17025. Preparation procedures are detailed on the Actlabs website (Activation Laboratories Ltd. 2014). Powdered and fused samples were analyzed by Perkin Elmer Sciex ELAN 6000, 6100 or 9000 ICP/MS, and samples from each core were randomized prior to analysis. Three blanks and five controls (three before the sample group and two after) also were analyzed per group of samples. Control samples included standards NIST694, DNC-1, and BIR-1a for major elements, and OREAS 100a and 101a, NCS DC 86312, 70009, and 70014 for minor and trace elements. The relative standard deviation from replicate analyses of the standard is <5% for major elements and <10% for minor/trace elements. The uncertainty associated with various determinations is ± 100 % at the detection limit (DL), ± 15 % at x10 DL and ± 5 % at x100 DL. Duplicates were fused and analyzed every 15 samples with instrument recalibration after every 40 samples.

Analyses of the different cores were run several months apart. Although the same standards were run with each analysis, and quality control checks indicate consistent readings, during statistical analyses we follow Tuttle *et al.* (1983) and do not combine data from different cores into single datasets.

In whole-rock geochemical data, variables are non-negative and compositional in nature; values are recorded as a proportion of the whole, i.e., ppm or percent (%). This constrained sample space, or the simplex, leads to what is known as the constant sum problem, which together with an often non-normal distribution of the data, makes basic statistical analyses (e.g., variance, correlation, regression and its derivatives) inapplicable (Pearson 1896; Chayes 1960; Butler 1979; Davis 2002). It also means that the compositional variables are, in fact, ratios whose denominators are rarely the sum of all the constituents available to be measured (Davis 2002). To overcome this problem, Aitchison (1986) demonstrated that centred log ratio (CLR) data transformation allows for the use of standard statistical methods on such geochemical data (Can Mert *et al.* 2016). This transformation is a simple process done by taking the natural log of each quotient where each compositional variable is divided by the geometric mean of the composition. Elements with more than one recorded value below detection limit remain problematic. For elements with only one such value (cobalt, zinc, germanium, tin, thallium), an artificial value (v) was assigned for statistical purposes, where v = x – (x/10) and x = detection limit (Davis 2002). Elements with more than one value below detection limit were excluded from statistical analyses. The raw data (in ppm) are provided in Appendix A.

SEDIMENTOLOGY

Sedimentological analysis of red bed cores taken from most of the recent vertical PCS exploration boreholes (Figs. 1c, 3, 4) resulted in the identification of 11 major lithofacies (Table 1). Lithofacies are mainly reddish-brown, pale brown, brownish-grey, and brown; ferruginous or calcareous; and mainly horizontally stratified. A unique bluish- or brownish-grey sandstone interval containing rip-up clasts and/or plant fragments occurs in the lower parts of most boreholes. The summary sedimentological logs (Fig. 3) indicate that fine-grained and/or sandstone-dominated facies broadly coarsen upward to gravel facies, with the amount of coarse-grained sediment also increasing toward the northeastern part of the study area. Accordingly, four intervals, the lower red sandstone-siltstone interval, bluish-grey sandstone interval, upper red sandstone-siltstone interval, and red polymictic conglomerate interval, have been identified. They are briefly reviewed in terms of their lithofacies associations. Also for brevity, since limited information is preserved in core (e.g., lateral facies relationships and larger scale geometries are not present to narrow down an interpretation), a plethora of possible conditions exist under which these various sedimentary structures are deposited, and a comprehensive discussion of all the possible interpretations is not feasible: only our favoured interpretations are presented.

Lower red sandstone-siltstone interval

Description: This interval comprises pale brown to greyish-brown, very fine- to fine-grained sandstone and siltstone, with rare scattered thin greenish- or bluish-grey bands and blotches. The beds were observed to have dips of ~5 to ~20 degrees. The maximum core thickness of this interval is ~220 m in PCS-05-04 (in the southwestern part) with a minimum thickness of ~97 m in PCS-04-01 at the northeast corner of the study area. Packages of sandstone beds range in thickness from ~0.5 m to ~27 m, and siltstone packages from ~2 m to ~33 m. Individual packages both coarsen and fine upward; however, the interval shows an overall coarsening-upward trend (except PCS-02-04). The most commonly identified lithofacies are Sh, Sx, Sp, Fl, and Fm, with lithofacies St, Sm, and Fd subordinate. Scattered nodular carbonate and sulfate concretions are also present. Cross-laminations in lithofacies Sx are mostly asymmetric and rarely display climbing. Mudstone rip-up clasts, identified in places in sandstone packages, are light brown to dark brown, subangular to subrounded, and elongate. Such clasts may also be present in rare, thinly interbedded polymictic conglomerate of core from the northeastern boreholes.

Interpretation: The colour of the intercalated sandstone and siltstone unit is evidence of subaerial exposure and a low water table in a predominantly oxidizing environment (Walker 1967; Abdul Aziz *et al.* 2003; Spalletti and Pinol 2005). Horizontally stratified sandstone (Sh) is interpreted as evidence of high energy flow (i.e., upper plane bed), probably associated with flooding events (Miall 1977; Khalifa *et al.* 2006; Türkmen *et al.* 2007). Cross-stratified facies (i.e., Sx, Sp, and St) commonly indicate the waning stage of flooding and decreasing velocity of flows towards lower flow regime conditions (Spalletti and Pinol 2005; Khalifa *et al.* 2006; Hadlari *et al.* 2006). Asymmetric current ripples were produced by unidirectional current (Chakraborti *et al.* 2009; Köykkä 2011), and the climbing shape of these ripples indicates high rates of aggradation (Collinson 1996). Fine-grained facies (i.e., Fl and Fm) represent deposition mostly from suspension (Hadlari *et al.* 2006; Köykkä 2011).

Structureless or massive sediments (i.e., Sm and Fm) are interpreted as having formed under conditions of high rates of suspension settling from currents of moderate to high sediment concentration (Abdul Aziz *et al.* 2003; Spalletti and Pinol 2005). Other possibilities exist but are less likely. For example, animals and plants are known to have colonized the local landscape by Mississippian times (e.g., Keighley and Pickerill 1994, 2003; Falcon-Lang 2004). Thus, massively bedded siltstones might indicate complete bioturbation of the substrate (Rhoads 1967), but there is no instance of partly bioturbated beds with distinct burrows or roots to suggest soil-forming activity, which would be an odd dichotomy.

Soft-sediment deformations (Fd) indicate release of excess pore-water pressure or dewatering (Spalletti and Pinol 2005). Siltstone rip-up clasts are interpreted as a record of high energy flooding and reworking of previously deposited mudstone (Spalletti and Pinol 2005; Köykkä 2011). Interbedded sandstone units indicate deposition from unidirectional water flow of both waning velocity (fining-up beds,

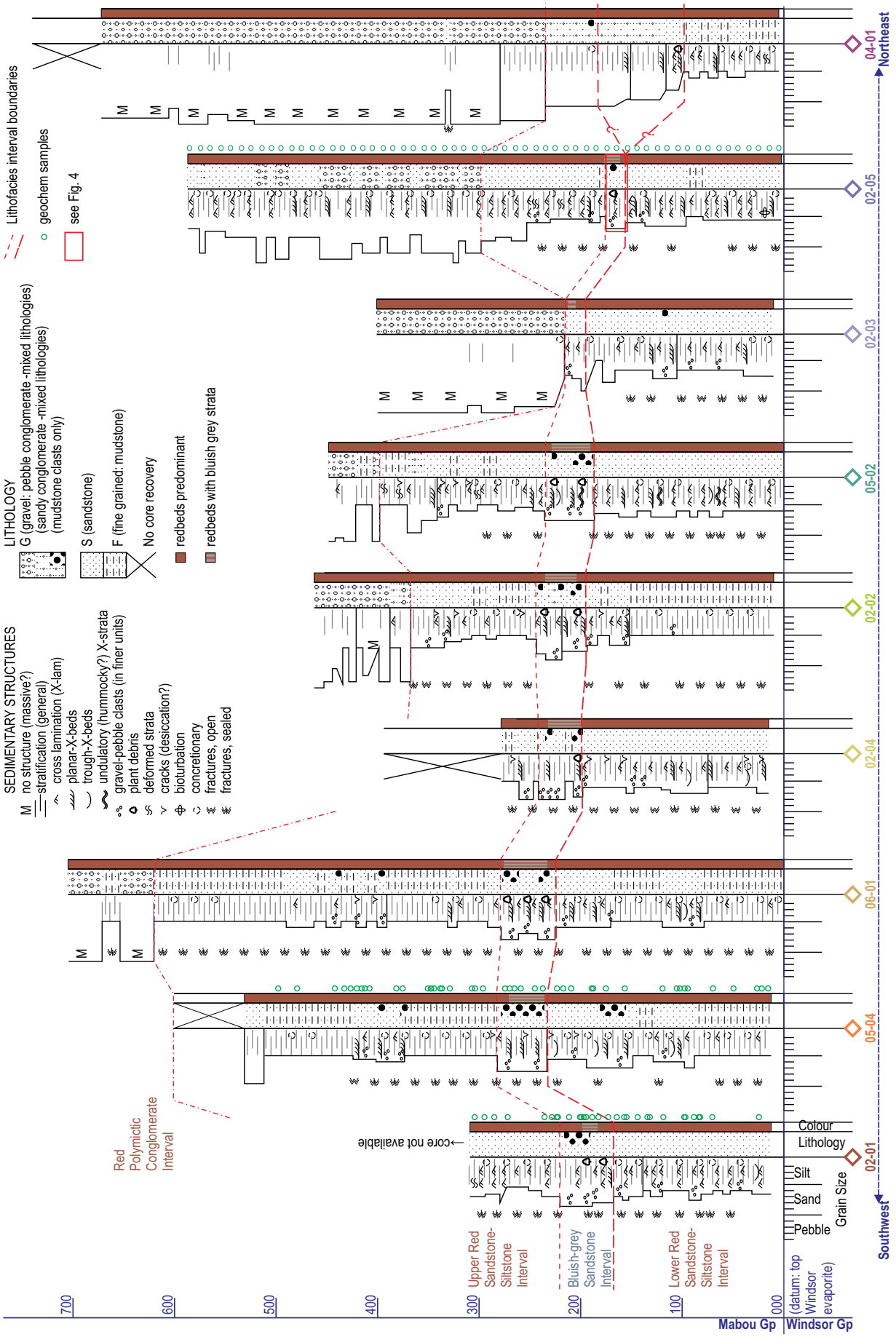

Figure 3. Generalized sedimentological logs of 9 boreholes from the vicinity of the Penobsquis PotashCorp mine. The bluish-grey sandstone interval consists of mudstone rip-up clasts and/or plant fragments. Scale in metres.

e.g., McEwen *et al.* 2011) and increasing velocity (coarsening-up beds, e.g., Heward 1978). The presence of siltstone rip-up clasts indicates downcutting into intraformational sediment, which could be considered evidence of upstream channelization. The small core diameter and many core breaks at the contact between sandstone and mudstone preclude confirmation of downcutting and channelization (i.e., fluvial flow). Although coarsening-upward profiles could represent, for example, prograding fan lobes, crevasse splays, or avulsion belts, they can also be related to base-level changes (Türkmen *et al.* 2007). Collectively this association of sandstone and intercalated siltstone favours a braidplain or distal alluvial fan setting. Laminated red bed mudstone, with rare nodular carbonate and sulfate but no bioturbation and rhizoconcretions, suggest harsh terrestrial conditions in the floodplain environment: regolith, but no paleosol, development.

Bluish-grey sandstone interval

Description: This interval is composed of gently dipping (up to 20 degrees) pale brown, brownish-grey, bluish-grey, or mottled grey-brown, occasionally pebbly, fine- to coarse-grained (dominantly medium-grained) sandstone and siltstone. Unlike the under- and overlying intervals, the grey strata may be metre scale in thickness. In the western part of the study area, the thickness of this interval is ~75 m in PCS-06-01 and PCS-02-04, but < 20 m in PCS-02-03 (middle part of the study area). The thickness of the measured sandstone packages range from ~0.5 m to ~12 m and siltstone packages range from ~1 m to ~4 m. Both coarsening- and fining-upward packages are identified (but rarely at the scale that can be illustrated in the summary logs, Fig. 3); however, the interval typically shows an overall coarsening-upward trend (only PCS-02-03 shows a distinct fining-upward trend). The major lithofacies identified are Sh, Sx, and Sp with Fl, St, Sd, and Fm as subordinates. Cross-laminations or ripple cross-laminations (Sx) are asymmetric in profile. Coalified plant fragments (Fig. 4b) are unique to sandstone of this interval, and they were observed in most cores (not PCS-05-04 and PCS-02-03). Except for PCS-02-03 and PCS-04-01 (northeastern part of the study area), some sandstone also contains mudstone rip-up clasts of a size that can exceed the diameter of the core. Where occurring discretely, these clasts are grey, light brown or dark brown, angular to subrounded, and typically elongate (Fig. 4d). Again, such clasts may also be one component of several in rare, thinly interbedded polymictic conglomerate that occurs in the northeastern boreholes.

Interpretation: Broadly, the lithofacies association in this interval is little different from that of the underlying lower red sandstone interval. However, the more extensive grey colour of sediment and the preservation of organic matter suggest waterlogged conditions were sufficiently prevalent that organic, likely plant, matter was preserved, and oxidation of iron did not progress far enough to form haematite (Wright and Sandler 1994; Collinson 1996; Abdul Aziz *et al.* 2003). However, no roots, burrows, or other clear indicators of palaeosol are present.

Across the study area, this interval can be considered to mark a shift to a more permanently high-water table and thus a relative rise in base level, but otherwise still a braidplain or distal alluvial fan setting. The cause of this rise may be the result of one or a combination of factors; rising lake or sea level (eustacy), tectonism resulting in either relative lake-/sea-level rise, or drainage basin reorganization, a wetter climate. This is further discussed below.

Upper red sandstone-siltstone interval

Description: This interval is of gently dipping (~5 to ~30 degrees), reddish-brown, pale brown, and brown, very-fine- to fine-grained sandstone and siltstone, with coarse-grained sandstone also present in PCS-02-05 and PCS-04-01. As in the lower interval, thin greenish- or bluish-grey bands and blotches are irregularly present. In the western part of the study area the interval is ~300 m thick (PCS-06-01), but much thinner (i.e., ~10 m in PCS-02-03, ~40 m in PCS-04-01) in the middle and northeastern parts of the study area. The thickness of the measured sandstone packages ranges from ~0.5 m to ~15 m. As previously, both coarsening- and fining-upward packages are identified. Similarly, the interval shows an overall coarsening-upward trend in most boreholes (Fig. 3). Sandstone predominates in most cores, except for PCS-06-01, PCS-05-04, and PCS-02-04 (western and southwestern part of the study area) where siltstone is dominant. In the sandstone, lithofacies Sh, Sx, Sp, and subordinate Sm are recognized; Fl, Fm, and subordinate Fd are the commonly identified lithofacies in the siltstone. Again, cross-laminations (Sx) are mostly asymmetric in shape, with climbing cross-laminations identified in PCS-02-01, PCS-06-01, and PCS-05-02. Mudstone rip-up clasts, identified rarely in sandstone packages and also in thinly interbedded polymictic conglomerate, are light brown to dark brown, subangular to subrounded, and elongate.

Interpretation: This interval is considered to be similar to the distal alluvial fan to floodplain facies association described for the lower red interval, and represent a return to arid, ephemeral flow conditions in the study area. However, predominance of siltstone in the western and southwestern parts of the study area is inferred to represent waning of flood flow followed by suspension deposition (Hadlari *et al.* 2006; Köykkä 2011).

Red polymictic conglomerate interval

Description: This interval is not recorded in logged cores from PCS-02-01 and PCS-02-04 (in the southwestern part), and increases in thickness to over 500 m in PCS-04-01 in the northeastern end of the study area (Fig. 3). The gently dipping beds (up to ~25 degrees) comprise conglomerate packages that are up to ~58 m thick, sandstone packages up

Figure 4. Images of PotashCorp core from the Penobsquis area of New Brunswick. All core is 2.25 inches diameter (for scale). (a) Example of a complete core interval through the Bluish-grey Sandstone Interval, borehole 02-05. (b) Abundant coalified plant debris preserved on bedding planes (broken core slabs) in the Bluish-grey Sandstone Interval, 02-01. (c) Calcite-sealed fractures and calcareous concretions within the Upper Red Sandstone-Siltstone interval, 02-01. (d) Detail of mudstone rip-up clasts from the area shown in the red rectangle in 4A.

to ~14 m thick, and siltstone packages up to ~7 m thick. As with the other intervals, both coarsening- (dominant in this case) and fining-upward sequences exist at different scales. The conglomerate is composed of granule- to pebble-sized, poorly sorted, subangular to subrounded polymictic clasts. Felsic igneous rocks and metamorphic rocks (e.g., schist, gneiss) are the most commonly identified clast types; mudstone clasts also occur. Matrix-supported conglomerate predominates over clast-supported conglomerate (only identified in PCS-02-03, PCS-02-02, and PCS-05-04). The conglomerate matrix typically consists of reddish-brown to pale brown and medium- to very-coarse-grained sandstone. The commonly identified lithofacies within this interval are Gmg, Gcm, and Sh; subordinate lithofacies are Sx, Sp, and Fm. Asymmetric cross-laminations or ripple cross-laminations (Sx) were identified only in PCS-02-05 and PCS-05-02.

Interpretation: Matrix-supported conglomerate (Gmg) indicates deposition from debris flows where they moved as dense masses and the matrix strength was large enough to transport the clasts (Blair and McPherson 2009). Clast-supported conglomerate (Gcm) is also considered the product primarily of debris flows, rather than fluvial flow, because of the combined lack of imbricate pebbles, cross stratification, and erosion surfaces within beds (Blair and McPherson 1992; Martins-Neto 1996; Sohn *et al.* 1999), although these absences might simply be a function of observations being restricted by the narrow core diameter. The angularity of the clasts indicates deposition probably close to the source (Köykkä 2011). The poor sorting and polymictic nature indicate that there were a variety of sources for the clasts (Veevers *et al.* 2007). Gravel beds separated by discontinuous lithofacies Sh, Sp, and Sx indicate that deposition of the

sand occurred within gravel frameworks by sediment-laden aqueous currents (Hadlari *et al.* 2006). Rare fine-grained sediment (Fm) suggests that distinct flow events alternated with low energy fallout deposits of episodic floods (Spalletti and Pinol 2005). Thicker bedded conglomerate to the northeast indicates that the alluvial fan apex was located in this direction. Overall coarsening- and thickening-upward sequences suggest active alluvial fan progradation and outbuilding (Heward 1978; Türkmen *et al.* 2007).

CHEMOSTRATIGRAPHY

The grey sandstone interval is a distinct stratigraphic marker in the study area, the base of which, as interpreted, marks a shift in depositional conditions. The bulk geochemical data collected (from PCS-02-01, PCS-05-04, and PCS-02-05) can be used to statistically test whether the base of the grey sandstone interval is also a distinct chemostratigraphic horizon. Simply, for comparison of variances and mean values, the null hypothesis can be tested against its opposite:

$$H_o{:}H_{\text{upper interval}} = H_{\text{lower interval}} \text{ against}$$
$$H_1{:}H_{\text{upper interval}} \neq H_{\text{lower interval}}$$

where below the base grey sandstone interval is considered as 'lower interval', and the base grey sandstone interval and above are considered as 'upper interval'. Significance was set at $\alpha = 0.05$ in all analyses. Differences in correlation coefficients and simple regression equations (with SiO_2 as the explanatory variable) provide additional comparisons.

Geochemical data can be presented in different ways, including simple plots of specific elements against depth or location, and scatter plots (Harker diagrams and discriminant plots) of two elements or two computed groups of elements, e.g., to identify provenance. In the selected plots presented herein (Figs. 5 to 9), data from the lower interval are coloured blue, and data from above the base of the grey sandstone interval are coloured red.

Provenance

Results: The provenance diagrams of Roser and Korsch (1988) were developed from a principal component analysis of several major elements measured from sandstone and mudstone of readily determinable provenance. The plots of provenance for the Sussex boreholes indicate that the red beds are of mixed quartzitic, felsic, and rare intermediate source (Fig. 5). They also suggest a difference between upper and lower interval samples. Materials from the lower interval are more tightly constrained and plot to the lower right of the data from the upper interval. The plots also suggest that the distinction might be most pronounced in the material from core PCS-02-05. It appears that these provenance graphs were first constructed using non-transformed data and so statistical analyses to test the similarity of upper and lower intervals were not performed using our data. Instead, the suggestion of a difference between the upper and lower interval is further investigated using transformed (centered log ratio) data of paired elements below. These further investigations are undertaken critically because Pe-Piper *et al.* (2008) noted that bulk geochemical approaches to provenance analysis of the terrigenous sedimentary rocks lack a globally applicable set of element discriminants.

Interpretation: The provenance plots are indicative of a more restricted suite of minerals, which consist of a higher mafic component, in the lower interval relative to the upper interval. Also, such a distinction may be more pronounced in the more proximal, NE part of the study area.

SiO_2:Al_2O_3

Results: For SiO_2 plotted against Al_2O_3, the raw data from the Sussex boreholes indicate that Si and Al are the two dominant elements, representing between 65% and 85% of the total composition (Fig. 6a). The four outliers, from PCS-05-04, represent the samples with the highest Ca abundance. For the transformed data, a significant difference in the variance of the Si:Al ratios between the upper and lower intervals is identified only in PCS-02-05 (all lithologies combined, Fig. 6c). However, with the exception of the upper interval in PCS-02-05, there is a significant negative correlation both in the upper and lower intervals. A similar pattern is present when the data are subdivided on lithologic character (Figs. 6d to k). The random sampling program did not result in sufficient mudstone samples for statistical analysis.

Interpretation: Silica (Si) and aluminum (Al) are major elements in many of the same common sedimentary minerals, in a ratio of ~3:1 for K-feldspars and ~1:1 for anorthite or kaolinite. A mix of kaolinite and K-feldspar, or of other clays and micas (typically also with Si:Al ratios between 3:1 and 1:1) in different samples would give increasing scatter somewhere between 3:1 and 1:1. However, some common Si-bearing minerals lack Al, e.g., quartz, zircon, and titanite. Samples also containing an increasing proportion (with respect to the Al-silicates) of these latter minerals would plot closer to the Si axis and produce even greater scatter. Therefore, viewing the data as a whole, the red beds can be considered a mix primarily of Si-minerals and subordinate alumino-silicate minerals.

Elemental abundances are typically reported as weight

Figure 5. (next page)+ Classification plots of discriminant functions F1 ($-1.773TiO_2 + 0.607Al_2O_3 + 0.76Fe_2O_3$ (T) $- 1.5MgO + 0.616CaO + 0.509Na_2O - 1.224K_2O - 9.09$) and F2 ($0.445TiO_2 + 0.07Al_2O_3 - 0.25Fe_2O_3$ (T) $- 1.42MgO + 0.438CaO + 1.475Na_2O + 1.426K_2O - 6.861$) for the red beds in the study area. Data indicate mixed quartzitic, felsic and rare intermediate sources. Provenance fields are from Roser and Korsch (1988).

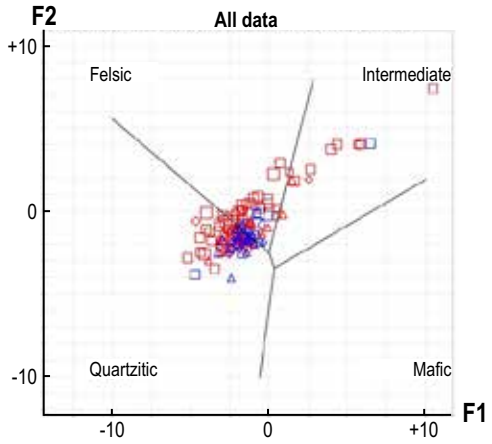

Legend

- lower, 02-01, sandstone
- lower, 02-01, mudstone
- upper, 02-01, sandstone
- upper, 02-01, mudstone
- upper, 02-05, conglomerate
- lower, 02-05, sandstone
- upper, 02-05, sandstone
- lower, 02-05, mudstone
- upper, 02-05, mudstone
- lower, 05-04, sandstone
- upper, 05-04, sandstone
- lower, 05-04, mudstone
- upper, 05-04, mudstone

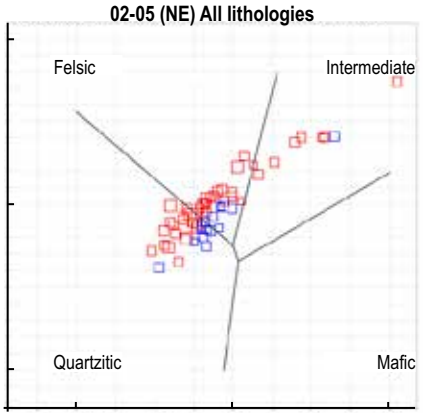

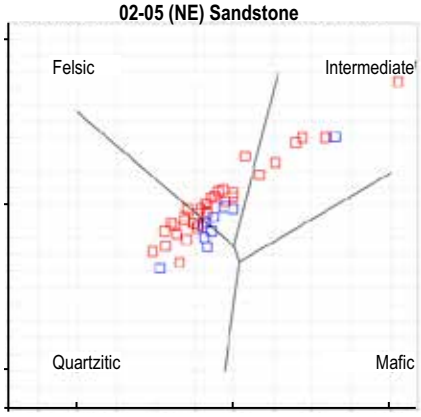

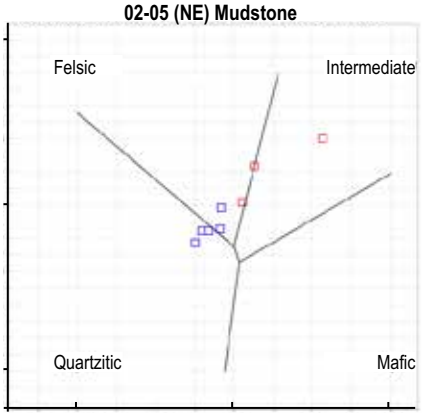

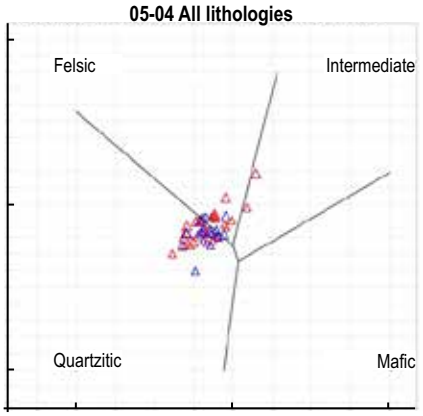

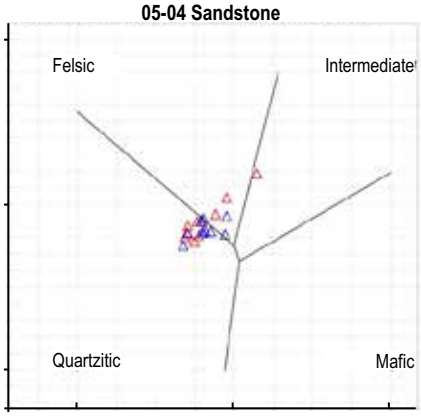

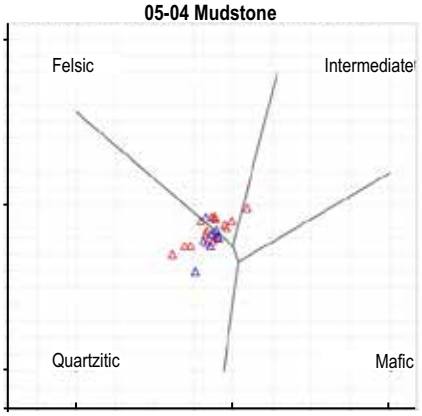

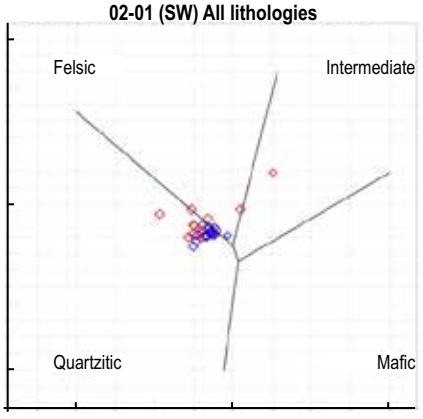

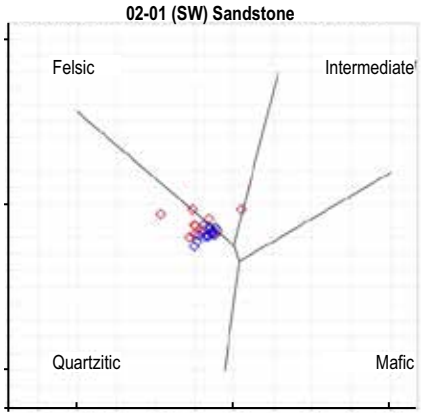

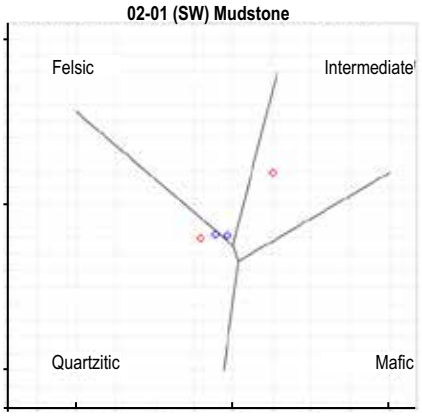

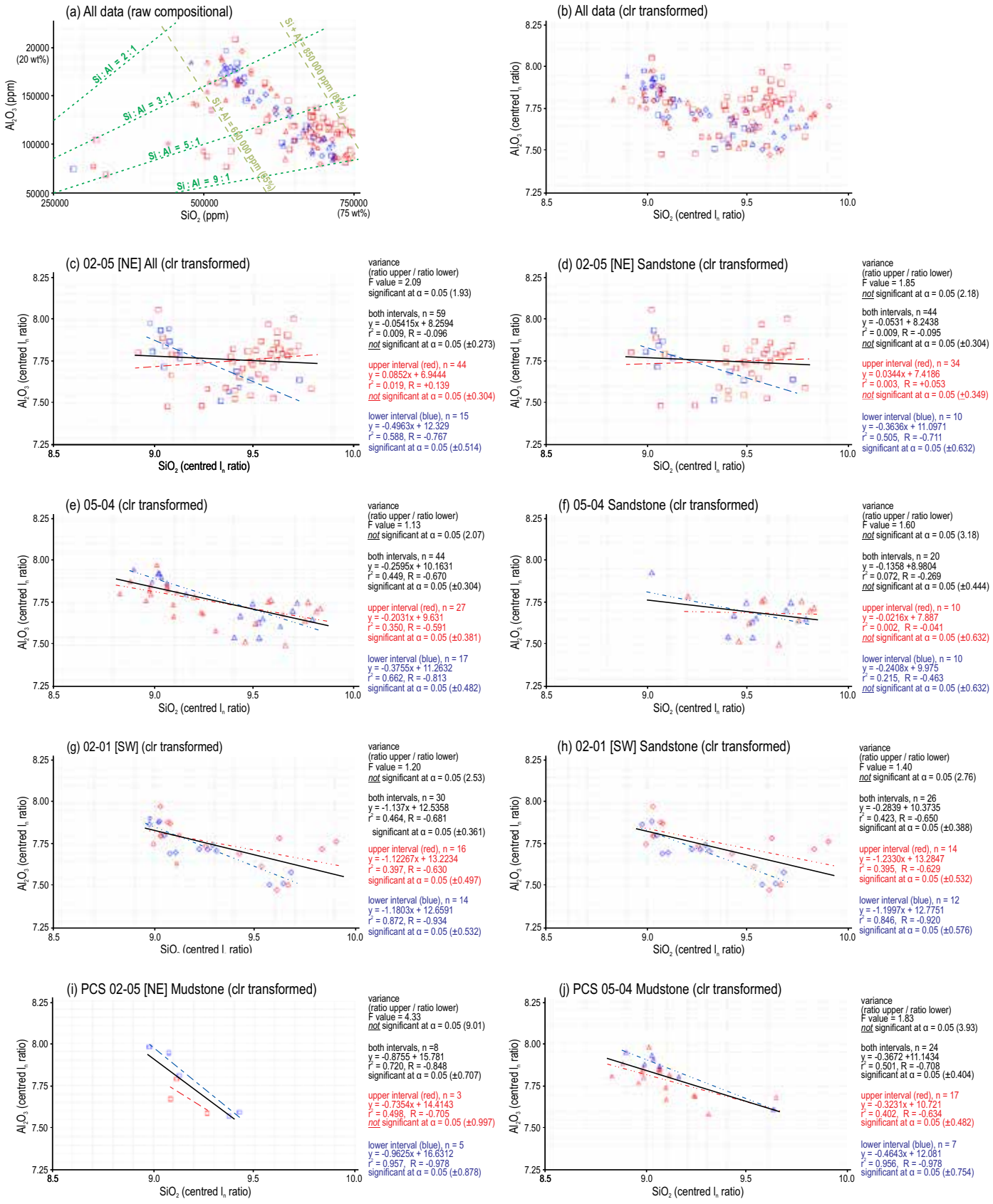

proportions (in % or ppm), and so are subject to the constraint: $x_{Si} + x_{Al} (\ldots + x_{D}) = 100\%$ (Aitchison 1986). For non-transformed data, the sample space is confined below the negative gradient line of closure (Aitchison 1986), which in a plot of Si:Al runs from 0_{Si}:100_{Al} through to 50_{Si}:50_{Al}, (pure kaolinite or similar), and down to 100_{Si}:0_{Al} (pure silica).

Figure 6. (previous page and below) Plots of SiO_2 vs. Al_2O_3 indicating that variances are not significant (except PCS-02-05) and correlations are mainly negative. Symbols area as in the legend for Figure 5. Abbreviations: F= variance statistic, n= number of samples analyzed, r^2= coefficient of determination, R= correlation coefficients, and α= values of significance.

Different abundances of (alumino-) silicates in the samples trend left and below the closure line. Accordingly, even though it is likely Al always positively associates with Si (i.e., Al always occurs in an alumino-silicate mineral), the closure effect in a compositional dataset promotes a negative association between these two predominant elements (Davis 2002): any increase in the amount of quartz must correspond to a decrease in the amount of alumino-silicate.

As noted in the sedimentology, the upper interval contains more abundant coarser-grained lithologies. This is a potential source of bias, as quartz tends to concentrate in the coarser fraction (Korsch *et al.* 1993). But samples above and below the base of the grey interval exhibit a negative gradient, indicating that both high and low Si:Al ratios occur throughout the succession. Most importantly, the transformed data (Fig. 6) display more limited scatter about the regression line and significant negative correlations for the lower samples compared to the upper interval. Although the trend is not ubiquitous, it suggests less variable compositions and fewer minerals in the lower interval in all wells, regardless of grain size.

K_2O:Na_2O

Results: When Na_2O is plotted against K_2O, no significant variances are noted. For all lithologies (Figs. 7c, e, g) there is a significant negative correlation to the data in the lower and upper intervals for all three boreholes, with Na content typically being less in the lower interval of each borehole. The same pattern is present in plots of sandstone lithologies (Figs. 7d, e, h), although correlations are significant in all cases except for the upper interval of PCS-05-04.

Interpretation: The Na_2O vs. K_2O scatter plot is commonly used in chemostratigraphic studies, but typically with K and Na expressed as ratios of Ti (whereby spurious correlations can be created if the data have not been transformed; Rollinson 1993; Davis 2002). The plot is generally considered to reflect the proportion of albite to anorthite feldspar, and of clay minerals montmorillonite to illite (Sabaou *et al.* 2009). Higher Na values in the upper interval suggest a greater ratio of albite (Na-rich) in the feldspar component and probably more mafic rock (e.g., gabbro and basalt) weathered in the source. As previously noted, for the major oxides, the effect of data closure is what controls the negative trend.

Nb:Ta

Results: Raw data show the ratio of Nb:Ta is ~15:1 (Fig. 8a). Significant variance in this ratio occurs between the upper and lower intervals in all wells (greater data spreads exist in the upper interval). However, there is only a significant positive correlation coefficient between the two elements in PCS-02-05 and for the lower interval in PCS-02-01 (for the plot of all lithologies, the three outliers of mudstone influence the significant correlation in PCS-05-04).

Interpretation: Nb and Ta are typically enriched in felsic igneous rocks (Yang *et al.* 2008) and these elements are known to substitute in rutile (Pearce *et al.* 2005; Meinhold, 2010; Tonje *et al.* 2013). Also, in silicic magma, the concentrations of Nb and Ta closely covary with the concentration of TiO_2 and the ratio of Nb/Ta decreases as the magmatic composition becomes less mafic and more silicic (Zhou *et al.* 2000). However, the variation in Nb should be considered when bulk geochemical data are analyzed in sandstone (Pe-Piper *et al.* 2008). In this study, for sandstone samples, variances are different between the upper and lower intervals indicating that the upper interval can have both more mafic and more silicic provenance components relative to the lower interval.

TiO_2:Cr

Results: When TiO_2 is plotted against Cr (Fig. 9), the raw data indicate that Cr values are never greater than ~1/60 TiO_2 values. Correlation coefficients are rarely significant (e.g., upper interval in PCS-02-01) because Cr shows little variation with respect to TiO_2. However, differences in the variance of the TiO_2:Cr ratio are significant in all wells, whether for all lithologies combined, or for sandstone only. Cr values are typically lower in the upper interval whereas TiO_2 values are more variable and decrease from northeast to southwest in the upper interval.

Interpretation: The ratio of Cr:TiO_2 in the estimated average composition (Lentz 2003) of continental crust (~1:53) and North American Shale Composition (~1:63) is compatible with the present observations. However, whole-rock concentrations of TiO_2 and Cr are controlled primarily by the abundances of the heavy minerals, e.g., chrome-spinel for Cr and rutile for TiO_2 (Preston *et al.* 1998; Pearce *et al.* 2005; Meinhold 2010; Ratcliffe *et al.* 2010; Tonje *et al.* 2013). Also, Cr is more likely associated with the mafic-derived heavy

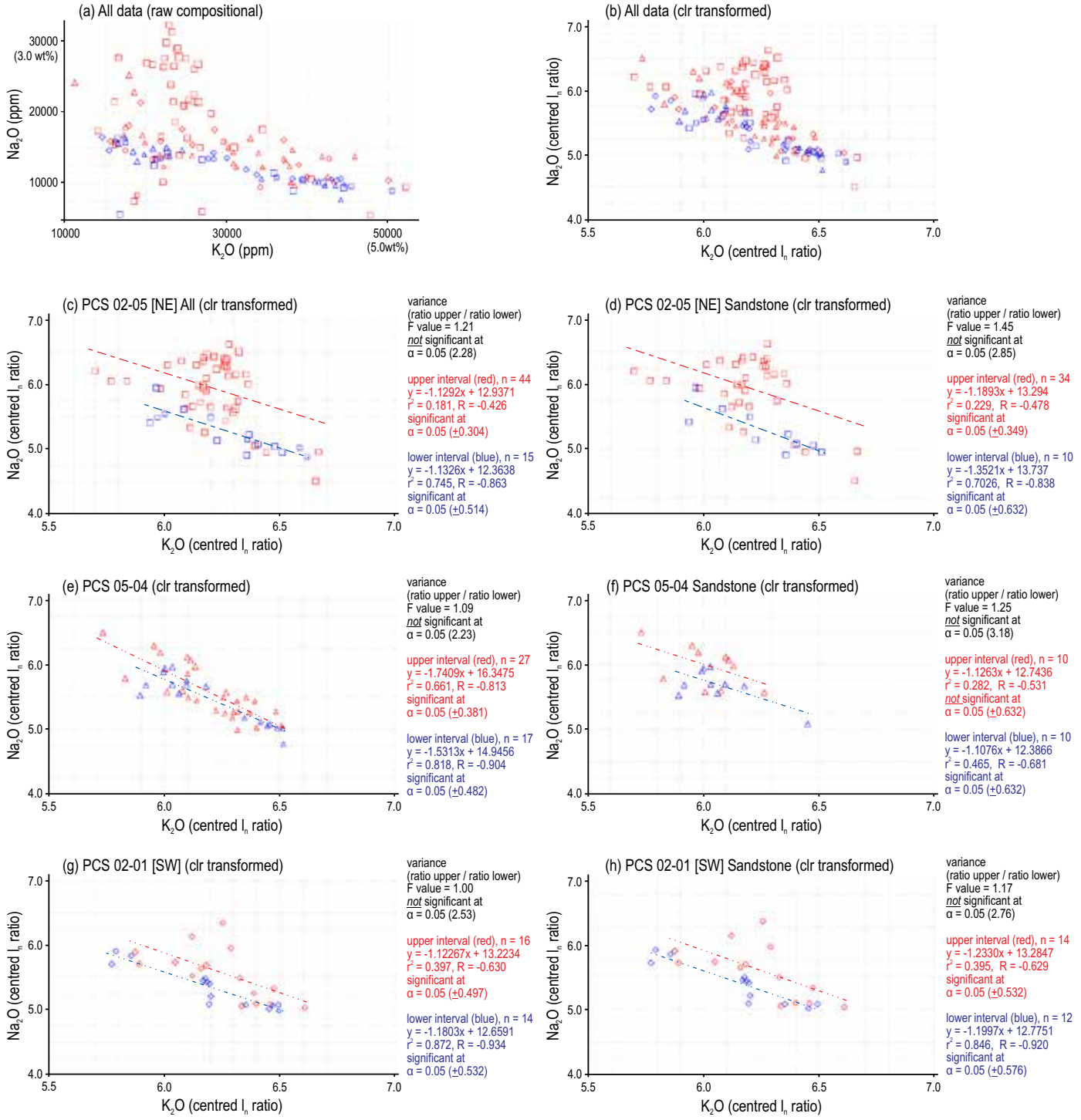

Figure 7. Plots of K_2O vs. Na_2O indicating that variances are not significant and negative correlations occur in all except F: sandstone in the upper interval of 05-04. Symbols are as in the legend for Figure 5. Abbreviations: F= variance statistic, n= number of samples analyzed, r^2= coefficient of determination, R= correlation coefficients, and α= values of significance.

minerals (Garver *et al.* 1996; Pearce *et al.* 1999; Ratcliffe *et al.* 2010). The concentration of TiO_2 is controlled by the composition of different types of magma (Ti more enriched in mafic magma) and TiO_2 tends to be enriched in the residual phases during weathering (Zhou *et al.* 2000). The absence of significant correlations suggests that elemental concentrations are not only a factor of the heavy mineral phase, but also of several other mineral phases, e.g., feldspars and clay minerals. Lower Cr values in the upper interval compared to the lower interval indicate that the upper interval had low to moderate mafic and more felsic influence in the source region. Variation in TiO_2 concentration in the upper

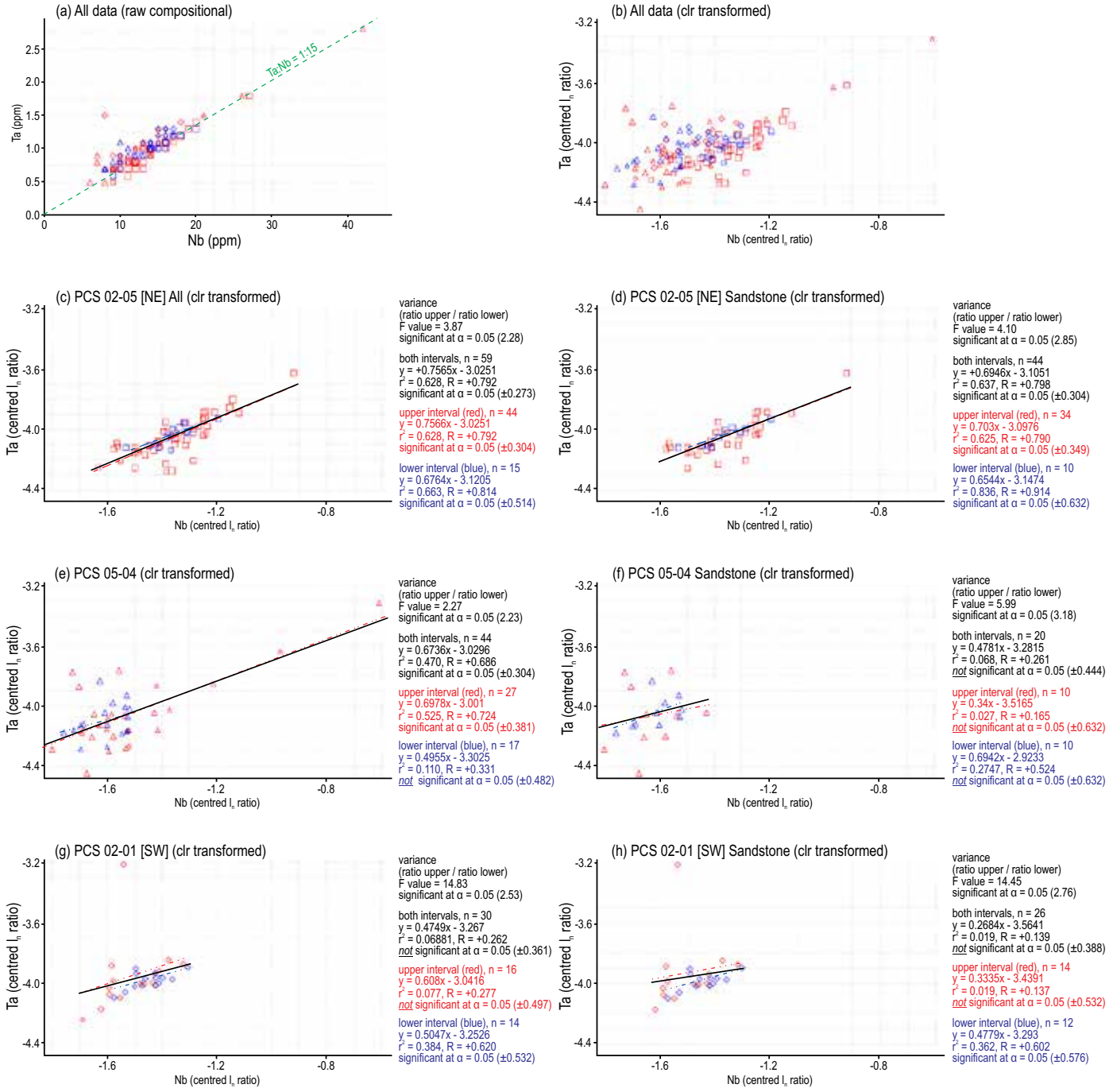

Figure 8. Crossplots of Nb vs. Ta indicating that variances are significant and where present, correlations are positive. Symbols are as in the legend for Figure 5. Abbreviations: F= variance statistic, n= number of samples analyzed, r^2= coefficient of determination, R= correlation coefficients, and α= values of significance.

interval may be due to the degree of mixture of varied source material or provenance change. Thus, the variability of Cr and TiO_2 is related to polycyclic origin, e.g., mixing of heavy mineral phases and sediment recycling. St. Peter and Johnson (2009) previously reported the presence of a Ti-Fe placer deposit ~25 km SE of Moncton in Hopewell Cape Formation (Mabou Group) strata, which they interpreted to reflect reworking of what would have been an uplifted, but now-buried, Ti deposit in Devonian(?) anorthosite.

DISCUSSION

The general lithofacies distribution in the studied boreholes suggests an alluvial fan to floodplain model, with the proximal fan located toward the northeast (Figs. 3, 10). Over time, the conglomerate units were able to prograde further toward the southwest. Of particular interest, however, is what we demarcate as the "bluish-grey interval", where exists a distinct combination of metre-scale bluish-grey beds

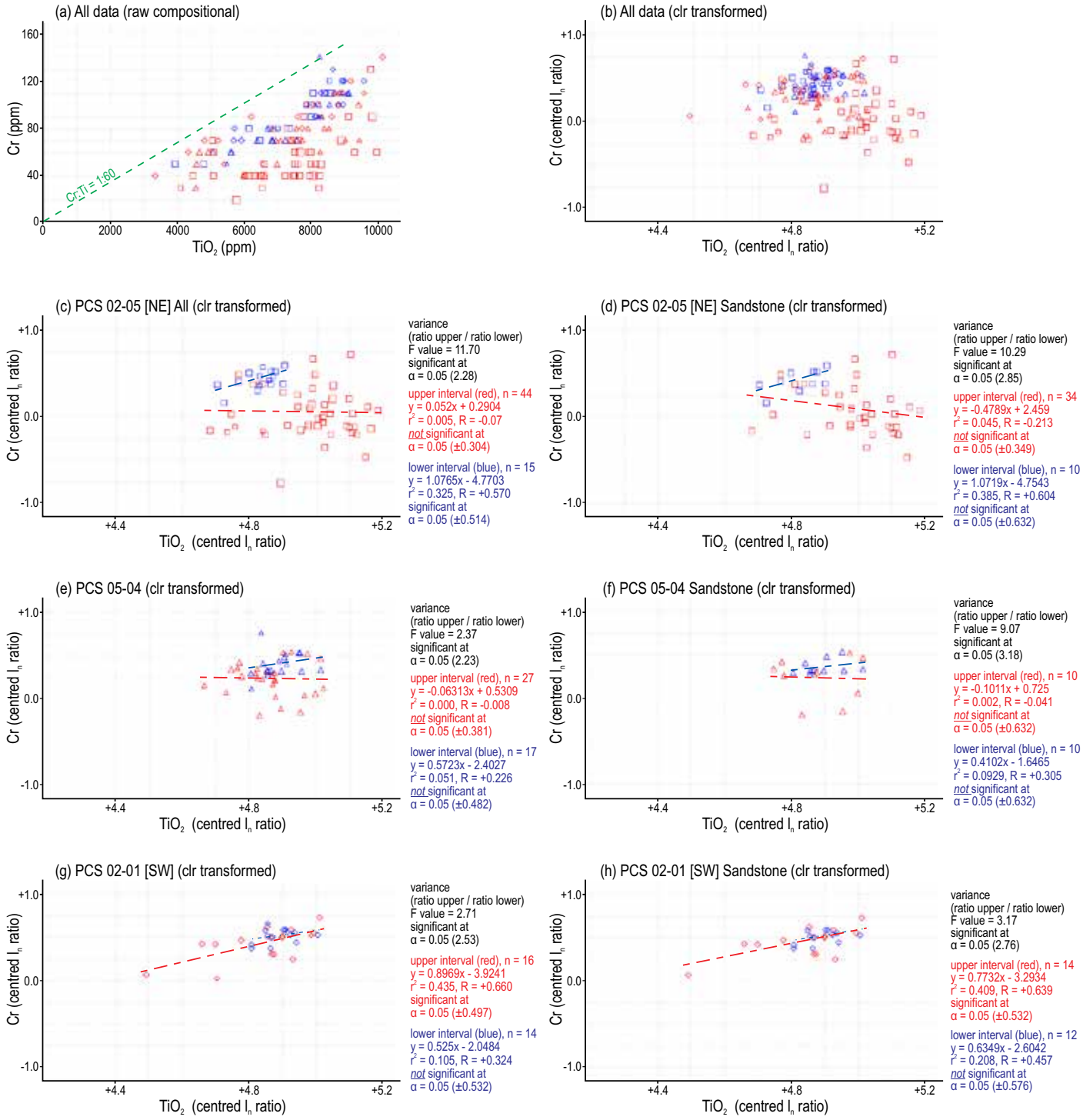

Figure 9. Crossplots of TiO_2 vs. Cr indicating that variances are significant and correlations are mainly not significant. Symbols are as in the legend for Figure 5. Abbreviations: F= variance statistic, n= number of samples analyzed, r^2= coefficient of determination, R= correlation coefficients, and α= values of significance.

of sandstone (non-red zones exist elsewhere but not at this scale), red or grey mudstone pebbles (i.e., rip-up clasts – also present, but to a lesser extent, at other stratigraphic levels) and, unique to this interval, plant detritus. As previously noted, preservation of plant fragments and patchy grey colouration indicate a more prevalent reducing environment. The presence of rip-ups suggests associated incision and reworking by channelization. This could be related to a rise in the water table (the terrestrial proxy for 'base level'), either related to relative sea- or lake level rise or simply a wetter climate resulting in more perennial discharge. The geochemical data above and below the base of the bluish-grey interval

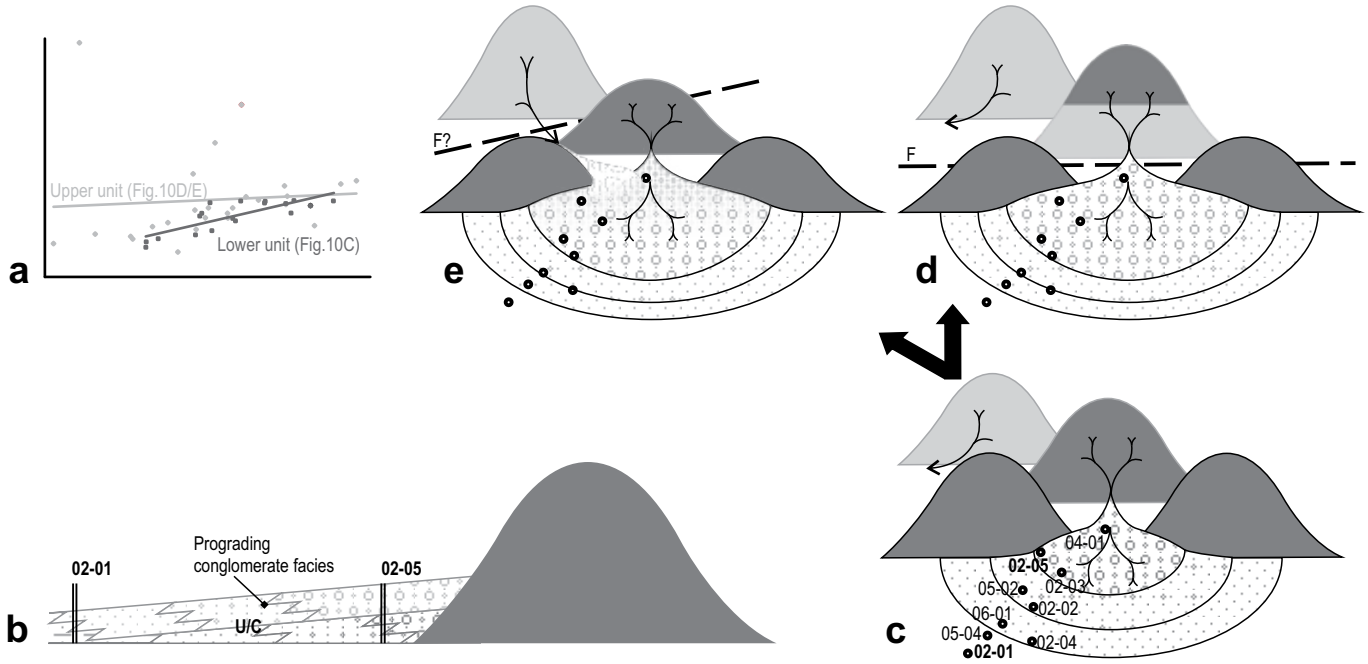

Figure 10. Schematic diagram illustrating depositional environments of the Mabou Group in the Sussex area. (a) Stylized graphical representation of data from the lower and upper units. (b) Schematic cross-section through the interpreted alluvial fan from distal (SW, borehole 02-01) to proximal (NE, borehole 02-05). (c) Early-Asbian: deposition of the lower red sandstone-siltstone interval. (d) Late-Asbian or younger: deposition of a more mineralogically varied upper red sandstone-siltstone interval due to uplift and exposure, erosion and transport of new rock types from the hinterland. (e) Late-Asbian or younger: deposition of a more mineralogically varied upper red sandstone-siltstone interval due to stream capture or expanded watershed resulting in erosion and transport of new rock types from the hinterland.

in addition indicate significant differences in the elemental compositions that likely reflect more varied provenance in the younger strata. This change could be due to gradual unroofing of additional rock types in the hinterland drainage basin.

In seismic profiles that cross the study area (Wilson and White 2005; fig 3b in Keighley 2008) a mid-Mabou angular unconformity, passing south into a (dis-) conformity can be picked, ~300–400 m above top Windsor, to the north of the subsurface Windsor-salt diapir (Fig. 1c). The Mabou Group is everywhere poorly imaged south of the diapir in the study area, but the bluish-grey interval might sit on the same unconformity south of the diapir. If so, rip-up clasts may be the result of vertical, rather than lateral, incision due to relative base-level fall; the reducing environment was potentially the result of base-level rise during subsequent infill of the incised valley. The lack of any distinct change in the dips of beds in PCS cores from above and below the base of the grey-coloured interval favours a disconformable contact, but the limitations of assessing minor changes in bedding from core material cannot rule out an angular boundary. Elemental geochemistry indicates a more varied suite of detrital minerals above the base grey-coloured interval (i.e., above the unconformity). This is indicated in the provenance plots and the goodness of fit to regression lines of Si:Al and K:Na, and statistically confirmed in f-tests of variance of Nb:Ta and Ti:Cr ratios between upper and lower intervals (Figs. 5 to 9). If tectonic uplift was involved in producing the unconformity, more varied source rocks could have been unroofed, weathered, and eroded from the hinterland. Alternatively, stream capture producing a larger hinterland exposing more varied lithologies may have resulted from uplift, or simply wetter climatic episodes, related to renewed relative base level rise following the development of the unconformity (Fig. 10).

Two different lithostratigraphic interpretations of the succession are possible. First, the grey sandstone interval, not previously recognized in outcrop in the Sussex area, may be considered equivalent to the Shepody Formation in the far southeast of New Brunswick. The lower red sandstone-siltstone interval would then be equivalent to the Middleborough Formation (syn. Maringouin Formation), and the upper red beds possibly equivalent to the Enragé Formation. In the type sections (southeastern New Brunswick), the thicknesses of the Maringouin, Shepody, and Enragé formations are ~496 to ~700 m, ~200 to ~330 m, and ~100 to ~150 m, respectively (St. Peter and Johnson 2009). If this interpretation is accepted, it would be the first indication in the Moncton Basin of a base-Shepody Formation disconformity, as Gussow (1953) previously identified an unconformity that he associated with the top of the formation. However, in contrast to the type sections, thicknesses of the equivalent 'formations' are quite different in the study area: ~220 to ~97 m, ~75 to ~7 m, and ~300 to ~10 m, respectively.

Alternatively, where the Windsor Group is more extensively exposed in Nova Scotia, five transgressive-regressive cycles are delineated (Giles 2009). Interfingering red bed intervals can be more than 250 m thick (Ryan and Boehner 1994), and a major unconformity is identified in the Asbian. Contrastingly, in the Moncton Basin, no late-Asbian (cycle II, e.g., Lime-kiln Brook Formation) and post-Asbian (cycle III to IV) Windsor Group carbonates or evaporites are known (St. Peter and Johnson 2009): the Lime-kiln Brook Formation is present only in the far SE part of New Brunswick in the Cumberland Basin (Fig. 2; Craggs *et al.* 2017). If the final marine regression of the Windsor Group sea in the Moncton Basin took place before the development of the Asbian unconformity, then an alternative lithostratigraphy for the Sussex area could be that the lower red bed unit, although by definition Mabou Group (lying above the uppermost preserved limestone), may be a Windsor Group cycle I landward equivalent. The capping grey sandstone and upper red beds would be cycle II transgression and regression equivalent or younger (Fig. 10), and strata equivalent to the Shepody Formation would, if ever deposited, overlie the studied section. Red beds disconformably underlying grey and plant-bearing sandstones have also been considered Windsor Group equivalent in Québec, where they have been assigned to the Percé Group (Jutras *et al.* 2001; Jutras and Prichonnet 2005). Although the latter interpretation is favoured, a final decision as to the most appropriate lithostratigraphy is still considered premature, because the unconformity has still not been mapped (and confirmed) in outcrop.

SUMMARY

One of the main constraints on previous studies of the red bed succession assigned to the Mabou Group of New Brunswick has been limited data due to poor outcrop exposure. However, access to nearly 5 km of recent drill cores from 11 boreholes has allowed sedimentological logging of several hundred metres of a continuous red bed succession. The succession can be divided into four intervals, i.e., the lower red sandstone-siltstone interval, bluish-grey sandstone interval, upper red sandstone-siltstone interval, and red polymictic conglomerate interval. The lower three intervals are interpreted as braidplain or distal alluvial fan deposits. The conglomerate interval indicates predominately debris flow alluvial fan deposits. The bluish-grey sandstone interval is associated with relative base level change that may simply be related to climate change or possibly to the development of a disconformity at its base.

A disconformity within post-Windsor Group red beds is supported by whole-rock geochemistry of 131 samples from three of the drill holes. Elemental variations observed through analysis of major element oxides and trace elements suggest a more varied or mixed provenance above the grey-coloured sandstone interval. For example, Nb:Ta and Ti:Cr ratios indicate a significant difference in the variance between upper and lower intervals.

ACKNOWLEDGEMENTS

PotashCorp, and particularly project contacts Brian Roulston, Arnfinn Prugger, and Colin MacDonald, are thanked for funding the study and for permission to publish. Activation Laboratories Ltd., Ancaster, Ontario, undertook the geochemical analyses. Two anonymous reviewers provided many constructive comments that have significantly improved the manuscript, which originated as the main part of the first-named author's M.Sc. thesis at the University of New Brunswick.

REFERENCES

Abdul Aziz, H., Sanz-Rubio, E., Calvo, J.P., Hilgen, F.J., and Krijgsman, W. 2003. Palaeoenvironmental reconstruction of a Middle Miocene alluvial fan to cyclic shallow lacustrine depositional system in the Calatayud Basin (NE Spain). Sedimentology, 50, pp. 211–236. https://doi.org/10.1046/j.1365-3091.2003.00544.x

Activation Laboratories Ltd., 2014. Methods. URL <http://www.actlabs.com/list.aspx?menu=64&app=226&cat1=549&tp=12&lk=no> June 2014.

Aitchison, J. 1986. The statistical analysis of compositional data. Chapman and Hall, London, 416 p. https://doi.org/10.1007/978-94-009-4109-0

Allen, J.P., Fielding, C.R., Rygel, M.C., and Gibling, M.R. 2013. Deconvolving signals of tectonic and climatic controls from continental basins: an example from the late Paleozoic Cumberland Basin, Atlantic Canada. Journal of Sedimentary Research, 83, pp. 847–872. https://doi.org/10.2110/jsr.2013.58

Anderle, J.P., Crosby, K.S., and Waugh, D.C.E. 1979. Potash at Salt Springs, New Brunswick. Economic Geology, 74, pp. 389–396. https://doi.org/10.2113/gsecongeo.74.2.389

Belt, E.S. 1964. Revision of Nova Scotia middle Carboniferous units. American Journal of Science, 262, pp. 653–673. https://doi.org/10.2475/ajs.262.5.653

Belt, E.S. 1965. Stratigraphy and paleogeography of Mabou Group and related middle Carboniferous facies, Nova Scotia, Canada. Geological Society of America Bulletin, 76, pp. 777–802. https://doi.org/10.1130/0016-7606(1965)76[777:SAPOMG]2.0.CO;2

Blair, T.C. and McPherson, J.G. 1992. The Trollheim alluvial fan and facies model revisited. Geological Society of America Bulletin, 104, pp. 762–769. https://doi.org/10.1130/0016-7606(1992)104<0762:TTAFAF>2.3.CO;2

Blair, T.C. and McPherson, J.G. 2009. Processes and forms of alluvial fans. Geomorphology of Desert Environments, Springer, Netherlands, pp. 413–467. https://doi.org/10.1007/978-1-4020-5719-9_14

Butler, J.C. 1979. Numerical consequences of changing the units in which chemical analyses of igneous rocks are analyzed. Lithos, 12, pp. 33–39. https://doi.org/10.1016/0024-4937(79)90060-4

Can Mert, M., Filzmoser, P., and Hron, K. 2016. Error

propagation in isometric log-ratio coordinates for compositional data: theoretical and practical considerations. Mathematical Geosciences, 48, pp. 941–961. https://doi.org/10.1007/s11004-016-9646-x

Chakraborti, P.P., Sarkar, A., Das, K., and Das, P. 2009. Alluvial fan to storm-dominated shelf transition in the Mesoproterozoic Singhora Group, Chattisgarh Supergroup, Central India. Precambrian Research, 170, pp. 88–106. https://doi.org/10.1016/j.precamres.2008.12.002

Chayes, F. 1960. On correlation between variables of constant sum. Journal of Geophysical Research, 65, pp. 4185–4193. https://doi.org/10.1029/JZ065i012p04185

Collinson, J.D. 1996. Alluvial sediments. *In* Sedimentary environments: processes, facies and stratigraphy. *Edited by* H.G. Reading. Blackwell Science, Oxford, pp. 37–82.

Craggs, S., Keighley, D., Waldron, J., and Park, A. 2017. Timing of salt tectonics affecting Pennsylvanian strata in the northern Cumberland Basin, SE New Brunswick, eastern Canada. Basin Analysis, 29, pp. 266–283.

Davis, J.C. 2002. Statistics and data analysis in geology, 3rd Edition. Wiley and Sons, New York, 638 p.

Falcon-Lang, H.J. 2004. Early Mississippian lycopsid forests in a delta-plain setting at Norton, near Sussex, New Brunswick, Canada. Journal of the Geological Society, London, 161, pp. 969–981. https://doi.org/10.1144/0016-764903-168

Force, E.R. and Barr S.M. 2006. A Lower Carboniferous two-stage extensional basin along the Avalon-Meguma terrane boundary: evidence from southeastern Isle Madame, Nova Scotia. Atlantic Geology, 42, pp. 53–68. https://doi.org/10.4138/2156

Garver, J.I., Royce, P.R., and Smick, T.A. 1996. Chromium and nickel in shale of the Taconic foreland: a case study for the provenance of fine-grained sediments with an ultramafic source. Journal of Sedimentary Research, 66, pp. 100–106.

Gibling, M.R., Calder, J.H., Ryan, R., van de Poll, H.W., and Yeo, G.M. 1992. Late Carboniferous and early Permian drainage patterns in Atlantic Canada. Canadian Journal of Earth Science 29, pp. 338–352. https://doi.org/10.1139/e92-030

Giles, P.S. 1981. Major transgressive-regressive cycles in middle to late Visean rocks of Nova Scotia. Nova Scotia Department of Mines and Energy, Paper 81-2, 27 p.

Giles, P.S. 2009. Orbital forcing and Mississippian sea level change: time series analysis of marine flooding events in the Viséan Windsor Group of eastern Canada and implications for Gondwana glaciation. Bulletin of Canadian Petroleum Geology, 57, pp. 449–471. https://doi.org/10.2113/gscpgbull.57.4.449

Gussow, W.C. 1953. Carboniferous stratigraphy and structural geology of New Brunswick, Canada. Bulletin of the American Association of Petroleum Geologists, 37, pp. 1713–1816.

Hadlari, T., Rainbird, R.H., and Donaldson, J.A. 2006. Alluvial, eolian and lacustrine sedimentology of a Paleoproterozoic half-graben, Baker Lake Basin, Nunavut, Canada. Sedimentary Geology, 190, pp. 47–70. https://doi.org/10.1016/j.sedgeo.2006.05.005

Hayward, N., Dehler, S.A., Grant, A.C., and Durling, P. 2014. Magnetic anomalies associated with salt tectonism, deep structure and regional tectonics in the Maritimes Basin, Atlantic Canada, 26, pp. 320–337. https://doi.org/10.1111/bre.12029

Heward, A.P. 1978. Alluvial fan sequence and megasequence models: with examples from Westphalian D-Stephanian B coalfields, Northern Spain. *In* Fluvial sedimentology. *Edited by* A.D. Miall. Canadian Society of Petroleum Geologists Memoir, 5, pp. 669–702.

Holt, N.M., García-Veigas, J., Lowenstein, T.K., Giles, P.S., and Williams-Stroud, S. 2014. The major-ion composition of Carboniferous seawater. Geochimica et Cosmochimica Acta, 134, pp. 317–334. https://doi.org/10.1016/j.gca.2014.03.009

Jutras, P. and Prichonnet, G. 2005. Record of late Mississippian tectonics in the new Percé Group (Viséan) of eastern Gaspésie, Québec. Canadian Journal of Earth Sciences, 42, pp. 815–832. https://doi.org/10.1139/e05-024

Jutras, P., Prichonnet, G., and Utting, J. 2001. Newly identified Carboniferous units (the Pointe Sawyer and Chemin-des-Pêcheurs formations) in the Gaspé Peninsula, Québec; implications regarding the evolution of the northwestern sector of the Maritimes Basin. Canadian Journal of Earth Sciences, 38, pp. 1–19. https://doi.org/10.1139/e00-073

Jutras, P., MacRae, R.A., and Utting, J. 2007. Viséan tectonostratigraphy and basin architecture beneath the Pennsylvanian New Brunswick Platform of eastern Canada. Bulletin of Canadian Petroleum Geology, 55, pp. 217–236. https://doi.org/10.2113/gscpgbull.55.3.217

Jutras, P., McLeod, J., MacRae, R.A., and Utting, J. 2016. Complex interplay of faulting, glacioeustatic variations and halokinesis during deposition of Upper Viséan units over thick salt in the western Cumberland Basin of Atlantic Canada. Basin Research, 28, pp. 483–506. https://doi.org/10.1111/bre.12119

Keighley, D.G. 2008. A lacustrine shoreface succession in the Albert Formation, Moncton Basin, New Brunswick. Bulletin of Canadian Petroleum Geology, 56, pp. 235–258. https://doi.org/10.2113/gscpgbull.56.4.235

Keighley, D.G. and Pickerill, R.K. 1994. The ichnogenus *Beaconites* and its distinction from *Ancorichnus* and *Taenidium*. Palaeontology, 37, pp. 305–337.

Keighley, D.G. and Pickerill, R.K. 2003. Ichnocoenoses from the Carboniferous of eastern Canada and their implications for the recognition of ichnofacies in nonmarine strata. Atlantic Geology, 39, pp. 1–22. https://doi.org/10.4138/1046

Khalifa, M.A., Soliman, H.E., and Wanas, H.A. 2006. The Cambrian Araba Formation in northeastern Egypt: facies and depositional environments. Journal of Asian Earth Sciences, 27, pp. 873–884. https://doi.org/10.1016/j.jseaes.2005.09.003

Korsch, R.J., Roser, B.P., and Kamprad, J.L. 1993. Geochem-

ical, petrographic and grain-size variations within single turbidite beds. Sedimentary Geology, 83, pp. 15–35. https://doi.org/10.1016/0037-0738(93)90180-D

Köykkä, J. 2011. Precambrian alluvial fan and braidplain sedimentation patterns: example from the Mesoproterozoic Rjukan Rift Basin, southern Norway. Sedimentary Geology, 234, pp. 89–108. https://doi.org/10.1016/j.sedgeo.2010.12.004

Lentz, D.R. 2003. Geochemistry of sediments and sedimentary rocks: historical to research perspectives. *In* Geochemistry of sediments and sedimentary rocks: Evolutionary considerations to mineral deposit-forming environments. *Edited by* D.R. Lentz. Geological Association of Canada, Geotext, 4, pp. 1–6.

Logan, W.E. 1845. Appendix W: Geological Survey. *In*: Appendix 1 to the Fourth Volume. Journals of the Legislative
Assembly of the Province of Canada, 1844(5).

Logan, W.E. 1864. Geological map of Canada. Geological Survey of Canada, Report of Progress from its commencement to 1863. Atlas of Maps and Sections, with an Introduction and Appendix, Montreal, 1865.

Lyell, C. 1843. On the coal formation of Nova Scotia and on the age and relative position of the gypsum and accompanying marine limestones. American Journal of Arts and Sciences, 43, pp. 356–359.

Martins-Neto, M.A. 1996. Lacustrine fan-deltaic sedimentation in a Proterozoic rift basin: the Sopa-Brumadinho Tectonosequence, southeastern Brazil. Sedimentary Geology, 106, pp. 65–96. https://doi.org/10.1016/0037-0738(95)00152-2

McCutcheon, S.R. 1981. Stratigraphy and paleogeography of the Windsor Group in southern New Brunswick. New Brunswick Department of Natural Resources, Mineral Resources Branch, Open File Report, 81-31, 210 p.

McEwen, L.J., Owen, G., Matthews, J.A., and Hiemstra, J.F. 2011. Late Holocene development of a Norwegian alpine alluvial fan affected by proximal glacier variations, episodic distal undercutting, and colluvial activity. Geomorphology, 127, pp. 198–215. https://doi.org/10.1016/j.geomorph.2010.12.016

Meinhold, G. 2010. Rutile and its applications in earth sciences. Earth-Science Reviews, 102, pp. 1–28. https://doi.org/10.1016/j.earscirev.2010.06.001

Miall, A.D. 1977. A review of the braided river depositional environment. Earth-Science Reviews, 13, pp. 1–62. https://doi.org/10.1016/0012-8252(77)90055-1

Miall, A.D. 1978. Lithofacies types and vertical profile models in braided river deposits: a summary. *In* Fluvial Sedimentology. *Edited by* A.D. Miall. Canadian Society of Petroleum Geologist Memoir, 5, pp. 597–604.

Miall, A.D. 1996. The Geology of Fluvial Deposits. Springer-Verlag, Heidelberg, 582 p.

Murphy, J.B., Waldron, J.W., Kontak, D.J., Pe-Piper, G., and Piper, D.J. 2011. Minas Fault Zone: late Paleozoic history of an intra-continental orogenic transform fault in the Canadian Appalachians. Journal of Structural Geology, 33, pp. 312–328. https://doi.org/10.1016/j.jsg.2010.11.012

Norman, G.W.H. 1941a. Hillsborough map sheet, Albert and Westmorland counties, New Brunswick. Geological Survey of Canada, Map 647A (with marginal notes).

Norman, G.W.H. 1941b. Moncton, Westmorland and Albert Counties, New Brunswick. Geological Survey of Canada, Map 646A (with marginal notes).

North American Commission on Stratigraphic Nomenclature, 1983. North American Stratigraphic Code. American Association of Petroleum Geologists, Bulletin, 67, pp. 841–875.

Park, A.F. and St. Peter, C.J. 2009. Stratigraphy and structure of the Indian Mountain Deformed Zone, Westmorland County, southeastern New Brunswick. New Brunswick Department of Natural Resources; Minerals, Policy and Planning Division, Mineral Resource Report 2009-1, 114 p.

Park, A.F., St. Peter, C.J., and Keighley, D.G. 2007. Structural styles in Late Devonian–Early Carboniferous rocks along the southern margin of the Moncton Subbasin: Caledonia Mountain to Elgin, southeastern New Brunswick. *In* Geological investigations in New Brunswick for 2006. *Edited by* G.L. Martin. New Brunswick Department of Natural Resources; Minerals, Policy and Planning Division, Mineral Resource Report 2007-1, pp. 87–125.

Park, A.F., St. Peter, C.J., Keighley, D.G., and Wilson, P. 2010. Overstep and imbrication along a sidewall ramp and its relationship to a hydrocarbon play in Tournaisian rocks of the Moncton Basin: the Peck Creek section, Albert Mines area, southeastern New Brunswick. Bulletin of Canadian Petroleum Geology, 58, pp. 268–282. https://doi.org/10.2113/gscpgbull.58.3.268

Pearce, T.J., Besly, B.M., Wray, D.S., and Wright, D.K. 1999. Chemostratigraphy: a method to improve interwell correlation in barren sequences—a case study using onshore Duckmantian/Stephanian sequences (West Midlands, U.K.). Sedimentary Geology, 124, pp. 197–220. https://doi.org/10.1016/S0037-0738(98)00128-6

Pearce, T.J., Wray, D.S., Ratcliffe, K.T., Wright, D.K., and Moscariello, A. 2005. Chemostratigraphy of the Upper Carboniferous Schooner Formation, southern North Sea. *In* Carboniferous hydrocarbon geology: the southern North Sea and surrounding onshore areas. *Edited by* J.D. Collinson, D.J. Evans, D.W. Holliday, and N.S. Jones. Yorkshire Geological Society, Occasional Publications Series, 7, pp. 47–164.

Pearce, T.J., Keighley, D.G., Morgan, T., and Flint, S. 2008. Chemostratigraphy in the Middle Member of the Green River Formation, Central Nine Mile Canyon, Southwest Uinta Basin, Utah. *In* Hydrocarbon systems and production in the Uinta Basin. *Edited by* M.W. Longman and C.D. Morgan. Rocky Mountain Association of Geologists and Utah Geological Association Publication, 37, pp. 121–132.

Pearson, K. 1896. Mathematical contributions to the theory of evolution. On a form of spurious correlation which may arise when indices are used in the measurement of organs. Proceedings of the Royal Society of London, 60,

pp. 489–502. https://doi.org/10.1098/rspl.1896.0076
Pe-Piper, G., Triantafyllidis, S., and Piper, D.J. 2008. Geochemical identification of clastic sediment provenance from known sources of similar geology: the Cretaceous Scotian Basin, Canada. Journal of Sedimentary Research, 78, pp. 595–607. https://doi.org/10.2110/jsr.2008.067
Preston, J., Hartley, A., Hole, M., Buck, S., Bond, J., Mange, M., and Still, J. 1998. Integrated whole-rock trace element geochemistry and heavy mineral chemistry studies; aids to the correlation of continental red-bed reservoirs in the Beryl Field, UK North Sea. Petroleum Geoscience, 4, pp. 7–16. https://doi.org/10.1144/petgeo.4.1.7
Ratcliffe, K.T., Wright, A.M., Hallsworth, C., Morton, A., Zaitlin, B.A., Potocki, D., and Wray, D.S. 2004. An example of alternative correlation techniques in a low accommodation setting, nonmarine hydrocarbon system: the (Lower Cretaceous) Mannville Basal Quartz succession of southern Alberta. Bulletin of the American Association of Petroleum Geologists, 88, pp. 1419–1432. https://doi.org/10.1306/05100402035
Ratcliffe, K.T., Wright, A.M., Montgomery, P., Palfrey, A., Vonk, A., Vermeulen, J., and Barrett, M. 2010. Application of chemostratigraphy to the Mungaroo Formation, the Gorgon Field, offshore Northwest Australia. Australian Petroleum Production and Exploration Association Journal 2010, 50th Anniversary Issue, pp. 371–385.
Rhoads, D.C. 1967. Biogenic reworking of intertidal and subtidal sediments in Barnstable Habor and Bazzars Bay, Massachusetts. Journal of Geology, pp. 461–476. https://doi.org/10.1086/627272
Rollinson, H.R. 1993. Using geochemical data: evaluation presentation, interpretation. Longman, England, 352 p.
Roser, B.P. and Korsch, R.J. 1988. Provenance signatures of sandstone-mudstone suites determined using discriminant function analysis of major-element data. Chemical Geology, 67, pp. 119–139. https://doi.org/10.1016/0009-2541(88)90010-1
Ryan, R.J. and Boehner, R.C. 1994. Geology of the Cumberland Basin, Cumberland, Colchester and Pictou Counties, Nova Scotia. Nova Scotia Department of Natural Resources, Mines and Energy Branches Memoir, 10, 222 p.
Sabaou, N., Ait-Salem, H., and Zazoun, R.S. 2009. Chemostratigraphy, tectonic setting and provenance of the Cambro-Ordovician clastic deposits of the subsurface Algerian Sahara. Journal of African Earth Sciences, 55, pp. 158–174. https://doi.org/10.1016/j.jafrearsci.2009.04.006
Sohn, Y.K., Rhee, C.W. and Kim, B.C. 1999. Debris flow and hyperconcentrated flood-flow deposits in an alluvial fan, northwestern part of the Cretaceous Yongdong Basin, central Korea. Journal of Geology, 107, pp 111–132. https://doi.org/10.1086/314334
Spalletti, L.A. and Pinol, F.C. 2005. From alluvial fan to playa: an Upper Jurassic ephemeral fluvial system, Neuquén Basin, Argentina. Gondwana Research, 8, pp. 363–383. https://doi.org/10.1016/S1342-937X(05)71141-2
St. Peter, C.J. 1993. Maritimes Basin evolution: key geologic and seismic evidence from the Moncton Subbasin of New Brunswick. Atlantic Geology, 29, pp. 233–270. https://doi.org/10.4138/2010
St. Peter, C.J. and Johnson, S.C. 2009. Stratigraphy and structural history of the late Paleozoic Maritimes Basin in southeastern New Brunswick, Canada. New Brunswick Department of Natural Resources; Minerals, Policy and Planning Division Memoir, 3, 348 p.
Stimson, M.R., Miller, R.F., Lucas, S.G., Park, A.F., and Hinds, S.J. 2016. Redescription of tetrapod trackways from the Mississippian Mabou Group, Lepreau Falls, New Brunswick, Canada. Atlantic Geology, 52, pp. 1–19. https://doi.org/10.4138/atlgeol.2016.001
Tonje, J.C., Ndjigui, P.D., Nyeck, B., and Bilong, P. 2013. Geochemical features of the Matomb alluvial rutile from the Neoproterozoic Pan-African belt, Southern Cameroon. Chemie der Erde – Geochemistry, 74, pp. 557–570.
Türkmen, İ., Aksoy, E., and Taşgin, C.K. 2007. Alluvial and lacustrine facies in an extensional basin: The Miocene of Malatya basin, eastern Turkey. Journal of Asian Earth Sciences, 30, pp. 181–198. https://doi.org/10.1016/j.jseaes.2006.08.006
Tuttle, M.L., Dean, W.E., and Parduhn, N.L. 1983. Inorganic geochemistry of Mahogany Zone Oil Shale in two cores from the Green River Formation. *In* Geochemistry and chemistry of oil shales. *Edited by* N. Miknis. American Chemical Society Symposium Series, 230, pp. 249–267. https://doi.org/10.1021/bk-1983-0230.ch013
Utting, J., Giles, P., and Dolby, G. 2010. Palynostratigraphy of the Mississippian and Pennsylvanian rocks, Joggins area, Nova Scotia and New Brunswick, Canada. Palynology, 34, pp. 43–89. https://doi.org/10.1080/01916121003620569
Veevers, S.J., Thomas, A.T., and Turner, P. 2007. Fan-delta sedimentation in the Silurian Coralliferous Formation of SW Wales: implications for the structure of the southern margin of the Welsh Basin. Geological Magazine, 144, pp. 319–331. https://doi.org/10.1017/S0016756806003013
Waldron, J.W.F., Rygel, M.C., Gibling, M.R., and Calder, J.H. 2013. Evaporite tectonics and the late Paleozoic stratigraphic development of the Cumberland basin, Appalachians of Atlantic Canada. Geological Society of America, Bulletin, 125, pp. 945–960. https://doi.org/10.1130/B30718.1
Waldron, J.W.F, Barr, S.M., Park, A.F., White, C.E., and Hibbard, J.P. 2015. Late Paleozoic strike-slip faults in Maritime Canada and their role in the reconfiguration of the northern Appalachian orogen. Tectonics, 34, pp. 1-24. https://doi.org/10.1002/2015TC003882
Walker, T.R. 1967. Color of recent sediment in tropical Mexico: a contribution to the origin of red beds. Geological Society of America Bulletin, 78, pp. 917–920. https://doi.org/10.1130/0016-7606(1967)78[917:CORSIT]2.0.CO;2
Webb, T.C. 2009. New Brunswick Potash: A review of Developments and Potential Exploration Alternatives. New Brunswick Department of Natural Resources; Minerals, Policy and Planning Division, Information Circular 2008-4 (CD-ROM), 21 p.
Wilson, P. 2005. Stratigraphy, structural geology and tecton-

ic history of the McCully area, Moncton Subbasin, southeastern New Brunswick. New Brunswick Department of Natural Resources; Minerals, Policy and Planning Division, Mineral Resource Report 2005-5, 104 p.

Wilson, P. and White, J.C. 2006. Tectonic evolution of the Moncton Basin, New Brunswick, eastern Canada: new evidence from field and sub-surface data. Bulletin of Canadian Petroleum Geology, 54, pp. 319–336. https://doi.org/10.2113/gscpgbull.54.4.319

Wilson, P., White, C.J., and Roulston, B.V. 2006. Structural geology of the Penobsquis salt structure: late Bashkirian inversion tectonics in the Moncton Basin, New Brunswick, eastern Canada. Canadian Journal of Earth Sciences, 43, pp. 405–419. https://doi.org/10.1139/e05-116

Wright, V.P. and Sandler, A. 1994. A hydrogeological model for the early diagenesis of Late Triassic alluvial sediments. Journal of the Geological Society, 151, pp. 897–900. https://doi.org/10.1144/gsjgs.151.6.0897

Yang, S., Yim, W.W.-S., and Huang, G. 2008. Geochemical composition of inner shelf Quaternary sediments in the northern South China Sea with implications for provenance discrimination and paleoenvironmental reconstruction. Global and Planetary Change, 60, pp. 207–221. https://doi.org/10.1016/j.gloplacha.2007.02.005

Zhou, Y., Bohor, B.F., and Ren, Y. 2000. Trace element geochemistry of altered volcanic ash layers (tonsteins) in Late Permian coal-bearing formations of eastern Yunnan and western Guizhou Provinces, China. International Journal of Coal Geology, 44, pp. 305–324. https://doi.org/10.1016/S0166-5162(00)00017-3

Editorial responsibility: Sandra M. Barr

Appendix A. Whole-rock chemical analyses of samples from drill cores.

Core/	core	core	core	core	core	core	core	core	core	core	core	core	core	core	core	core	core
Surface	02-01	02-01	02-01	02-01	02-01	02-01	02-01	02-01	02-01	02-01	02-01	02-01	02-01	02-01	02-01	02-01	02-01
Lithology	ss	st	ss	ss	ss	ss	ss	ss	ss	ss	ss	ss	ss	ss	ss	st	ss
depth	308	317	327	340	376	384	388	390	400	411	413	415	418	424	430	439	448
unit	upper	upper	upper	upper	upper	upper	upper	upper	upper	upper	upper	upper	upper	upper	upper	upper	lower
SiO_2	675200	441000	553900	617400	577300	487500	556200	577500	692700	748700	735800	687600	562900	712200	721700	599400	554400
Al_2O_3	120000	100800	162100	135600	176400	140800	162200	173300	80200	88300	89000	109900	196500	105100	85900	160800	177900
$Fe_2O_3^{(T)}$	55800	39200	74900	57100	81100	66000	80400	79400	33200	26800	32700	43900	49800	47300	39600	77700	80400
MnO	840	780	890	1110	680	630	600	600	990	620	680	530	450	610	870	470	540
MgO	18100	15900	29100	23600	25100	23000	24900	26700	10400	9700	11400	15000	30000	15800	12600	23300	24500
CaO	32200	129400	28400	33900	14300	73700	28700	16900	59900	38100	38900	28900	9800	30000	43800	10600	17200
Na_2O	15400	12300	16100	17500	10800	9500	10900	13500	15900	21300	18100	17600	10400	15900	14600	12600	10700
K_2O	25800	22200	37000	28500	42500	34100	39900	42600	15600	19400	17900	24500	50000	21800	17500	38900	44100
TiO_2	7550	5370	8600	7720	8930	7840	9160	8840	5200	3330	4320	4800	10120	7600	6200	9560	8690
P_2O_5	1100	1000	1400	1300	1100	1100	1300	1400	900	800	900	900	1500	1300	1200	1500	1000
LOI	53700	194800	77900	64700	65400	137500	70300	63200	75100	51600	50600	53100	66600	51500	54300	54400	71900
Sc	12	10	18	14	18	16	18	18	6	5	6	9	22	11	8	17	19
Be	2	2	3	2	3	2	3	3	1	1	1	2	4	1	1	3	3
V	73	62	133	95	133	109	136	132	47	36	48	60	159	77	56	139	137
Ba	318	383	505	374	443	337	368	417	463	394	336	719	443	270	634	382	550
Sr	155	732	259	143	159	148	119	102	255	131	119	409	92	88	173	89	216
Y	28	22	28	27	30	26	31	30	24	17	19	19	29	28	25	33	29
Zr	263	165	178	215	170	162	188	213	284	174	198	150	170	397	367	254	189
Cr	70	50	90	80	110	100	120	110	70	40	60	70	140	90	90	110	110
Co	13	9	21	16	21	17	18	17	6	5	7	9	25	10	8	16	19
Zn	90	90	140	120	150	110	120	130	60	50	60	80	120	70	70	110	140
Ga	16	13	22	18	25	20	25	23	11	12	12	15	29	15	12	22	25
Ge	3	1	3	2	3	3	3	3	2	2	2	2	3	2	2	3	3
Rb	93	85	137	106	167	135	154	161	57	80	64	88	184	84	65	145	163
Nb	13	9	14	12	16	14	16	15	9	8	8	9	18	13	10	16	15
Sn	3	3	4	4	5	4	5	5	3	6	3	3	6	4	3	5	5
Cs	5.3	4.6	8.8	6.6	10.3	8	8.7	9.4	2.4	3.6	2.8	4.3	10.3	4.1	3.2	8.3	9.8
La	32.1	27.8	33.2	32.1	42.6	42.2	45	39.9	24.9	20.7	23.5	25.7	50.7	33.3	29.6	44.8	47.2
Ce	62.4	55.9	66.2	66	85.5	85.8	91.2	78.8	52.2	39.6	46.2	49.2	95	67.2	61.3	88	92
Pr	7.05	6.39	7.57	7.58	9.28	9.19	10.1	8.9	6.33	4.59	5.37	5.68	9.99	7.78	7.18	9.99	9.85
Nd	27.1	25.2	29.7	30	35.6	33.9	38.3	33.2	25.5	18.5	21.2	22.7	37.3	30.7	29.3	37.7	36.3
Sm	5.7	5.1	6.5	6.4	7.1	6.5	7.3	6.9	5.8	4	4.5	4.9	6.9	6.5	6.2	7.9	6.9
Eu	1.25	1.07	1.41	1.35	1.59	1.35	1.57	1.47	1.14	0.85	1	1.08	1.47	1.31	1.26	1.65	1.41
Gd	5.2	4.2	5.9	5.4	6.1	5.2	6.3	5.9	4.8	3.2	3.9	4	5.7	5.3	5.3	6.6	5.6
Tb	0.8	0.7	0.9	0.9	1	0.8	1.1	1	0.7	0.5	0.6	0.6	0.9	0.9	0.8	1.1	0.9
Dy	4.8	3.9	5.4	5	5.7	5	5.9	5.4	4.2	2.9	3.5	3.7	5.5	5	4.5	6	5.2
Ho	1	0.8	1.1	1	1.1	1	1.2	1.1	0.8	0.6	0.7	0.7	1.1	1	0.9	1.2	1
Er	2.8	2.2	3.1	2.9	3.2	2.8	3.3	3.2	2.4	1.7	2.2	2.2	3.3	3	2.6	3.5	3.1
Tm	0.46	0.33	0.48	0.47	0.49	0.43	0.5	0.51	0.36	0.27	0.34	0.35	0.51	0.46	0.41	0.53	0.48
Yb	3.2	2.2	3.3	3.1	3.3	3	3.3	3.5	2.4	1.9	2.2	2.2	3.5	3.1	2.7	3.5	3.3
Lu	0.49	0.34	0.52	0.51	0.54	0.46	0.52	0.56	0.4	0.32	0.33	0.34	0.55	0.51	0.44	0.57	0.51
Hf	6.6	3.9	4.8	5.8	4.8	4.5	5.1	5.7	7	4.3	5	3.9	4.6	9.8	9	6.7	5
Ta	1	0.7	1.1	1	1.3	1.1	1.2	1.2	0.9	1.5	0.7	0.7	1.4	1.1	0.9	1.3	1.3
Tl	0.6	0.5	0.9	0.7	0.9	0.7	0.8	0.9	0.3	0.4	0.4	0.6	1.1	0.4	0.4	0.8	1
Pb	22	26	38	28	27	17	17	28	9	9	8	12	15	8	9	24	30
Th	9.6	7.3	10.9	10.1	13	11	12.3	13.1	7.8	5.9	6.7	7.5	14.5	10.1	8.8	13.1	13.2
U	2.4	2.1	3.4	3.1	3.3	2.7	4	3.4	1.9	1.4	1.6	1.8	4.1	2.6	2.2	3.3	3.1

Appendix A. Continued.

Core/	core	core	core	core	core	core	core	core	core	core	core	core	core	core	core	core	core
Surface	02-01	02-01	02-01	02-01	02-01	02-01	02-01	02-01	02-01	02-01	02-01	02-01	02-01	05-04	05-04	05-04	05-04
Lithology	ss	ss	ss	st	st	ss	ss	ss	ss	ss	ss	ss	ss	st	st	st	st
depth	455	457	468	478	480	494	514	515	524	529	530	542	588	287	306	342	352
unit	lower	lower	lower	lower	lower	lower	lower	lower	lower	lower	lower	lower	lower	upper	upper	upper	upper
SiO_2	714600	715600	543300	533000	549900	641800	590800	565800	619500	694700	639700	602100	618900	611000	641000	635400	687700
Al_2O_3	85400	88100	180100	182200	176200	129800	145500	163400	138300	88500	136800	151700	132100	157800	135500	113400	96900
$Fe_2O_3^{(T)}$	34800	34300	84700	91000	83600	58700	64000	72100	63000	36000	58400	65200	59900	66900	66100	51300	35800
MnO	990	880	600	640	620	860	830	670	740	1490	680	870	800	1130	780	870	1160
MgO	12000	12800	27500	28300	27000	20800	24100	27700	22400	14400	23100	25000	25900	27300	19700	16300	13500
CaO	53300	43500	19300	23900	20700	35300	40300	35100	33400	62800	28800	35100	33600	5700	15200	53500	51100
Na_2O	16000	16500	10400	9800	10600	13500	12000	10700	13600	14600	14300	11200	13400	10100	12300	13900	15700
K_2O	16200	14600	43600	44500	42900	27700	32400	38100	30000	15500	28400	33700	28400	37900	31200	25700	19900
TiO_2	5670	5690	9570	8630	8990	8120	8430	8940	8270	5900	8800	8930	8040	9010	9420	8260	5960
P_2O_5	1000	900	1300	1300	1200	1300	1300	1500	1400	1000	1300	1300	1100	1400	1400	1100	800
LOI	67900	58600	70000	74600	68800	63100	72500	74900	64500	72400	59400	71800	68600	54300	52100	64200	55200
Sc	8	8	20	20	20	14	16	18	15	9	14	16	14	16	14	11	9
Be	1	1	3	3	3	2	2	3	2	1	2	2	2	4	3	2	1
V	57	61	153	145	149	96	114	135	107	61	104	114	104	109	96	87	73
Ba	180	160	469	464	456	344	497	443	350	380	353	447	399	427	382	316	328
Sr	198	127	146	168	144	121	205	175	137	190	129	176	169	105	111	108	110
Y	25	23	30	29	29	29	29	29	28	26	29	31	28	40	33	33	24
Zr	412	325	169	159	165	228	208	180	233	253	238	271	221	318	390	387	258
Cr	70	80	120	130	120	90	110	120	110	70	100	100	100	70	70	60	40
Co	9	10	22	21	21	16	17	19	16	10	16	17	16	18	15	12	9
Zn	60	60	130	140	120	100	100	120	110	70	100	550	100	120	100	90	60
Ga	12	13	26	25	25	18	20	23	19	12	18	21	19	21	18	14	11
Ge	2	2	3	3	3	2	3	3	3	2	2	2	2	3	3	3	2
Rb	58	58	168	168	160	110	124	144	115	60	110	126	109	147	115	95	72
Nb	10	10	17	15	16	14	16	16	14	10	16	16	15	26	15	14	9
Sn	3	4	5	5	5	4	4	5	5	3	4	7	4	5	3	2	2
Cs	3	3	9.8	10.1	9.5	6.7	7.5	8.7	6.8	3.3	6.8	7.6	6.3	8.4	6.3	4.8	3.1
La	28.2	27.8	45.7	42.3	46.7	34.5	50.8	40.3	39.5	27.7	35.5	45.1	34.8	42.6	42.9	34.3	25.6
Ce	58.3	56.5	89.5	83.6	93.3	69.7	97.4	79.9	79.6	57.1	70.3	90.7	70	94.4	85.2	74	55.3
Pr	6.77	6.47	9.84	9.3	10.2	7.81	10.5	8.94	8.82	6.66	8.02	9.93	7.73	9.36	9.01	8.56	6.77
Nd	27.4	25.4	38.1	36.3	37.4	30.7	39.3	34.7	33.2	27.6	30.8	37.1	29.5	35.4	32.8	33.4	26.4
Sm	6.1	5.5	7.4	7.3	7.2	6.3	7.4	7.1	6.4	6.5	6.3	7	6.2	7	6.8	6.8	5.6
Eu	1.09	1.08	1.64	1.5	1.5	1.36	1.62	1.51	1.3	1.36	1.28	1.4	1.3	1.4	1.26	1.41	1.15
Gd	5	4.5	6.3	5.7	5.9	5.4	6.3	5.9	5.3	5.5	5.2	5.6	5.5	6.9	6	6.6	4.9
Tb	0.8	0.8	1	0.9	0.9	0.9	1	0.9	0.9	0.9	0.9	1	0.9	1.2	1	1	0.8
Dy	4.5	4.4	5.6	5.3	5.6	5	5.6	5.4	5.2	4.6	5.2	5.5	5	7.1	5.8	5.9	4.7
Ho	0.9	0.9	1.1	1	1.1	1	1.1	1.1	1.1	0.9	1.1	1.1	1	1.5	1.2	1.2	0.9
Er	2.6	2.5	3.2	3	3.2	2.8	3.1	3.1	3	2.5	3.1	3.1	2.9	4	3.5	3.4	2.4
Tm	0.4	0.37	0.5	0.47	0.48	0.44	0.47	0.48	0.45	0.39	0.48	0.49	0.45	0.63	0.55	0.51	0.38
Yb	2.7	2.5	3.4	3.2	3.1	3	3.2	3.2	3.1	2.7	3.3	3.3	3	4.1	3.8	3.4	2.6
Lu	0.43	0.42	0.55	0.52	0.5	0.48	0.51	0.51	0.5	0.43	0.51	0.55	0.47	0.65	0.61	0.51	0.39
Hf	10.1	8.2	4.6	4.4	4.6	5.9	5.5	4.8	5.9	6.3	6.4	6.9	5.9	7.5	8.5	8.6	5.7
Ta	0.8	0.9	1.3	1.2	1.3	1.1	1.2	1.2	1.1	0.8	1.2	1.3	1.1	1.8	1.3	0.9	0.7
Tl	0.3	0.3	0.9	0.9	0.8	0.7	0.7	0.8	0.7	0.4	0.6	0.7	0.6	0.9	0.6	0.5	0.4
Pb	10	8	33	30	23	24	30	28	24	12	20	53	20	30	31	25	14
Th	8.9	8.1	14	12.7	13	10.1	12.6	12.2	11.2	8.1	11.1	12.3	10.7	12.7	12	10.1	7.4
U	2.3	2.3	3.3	3.2	3.2	2.7	3.2	3.6	2.9	2.2	3.1	3.1	3	3	3	3.4	1.9

Appendix A. Continued.

Core/	core	core	core	core	core	core	core	core	core	core	core	core	core	core	core	core	core
Surface	05-04	05-04	05-04	05-04	05-04	05-04	05-04	05-04	05-04	05-04	05-04	05-04	05-04	05-04	05-04	05-04	05-04
Lithology	st	ss	ss	ss	st	ss	st	st	st	st	st	st	st	st	st	st	st
depth	359	365	369	373	377	403	409	435	437	438	441	447	448	456	478	481	489
unit	upper	upper	upper	upper	upper	upper	upper	upper	upper	upper	upper	upper	upper	upper	upper	upper	upper
SiO_2	561500	666800	682500	619800	607000	634700	554400	505600	532500	527900	482400	536200	505000	581400	550400	509100	529700
Al_2O_3	167200	109000	111200	150700	130200	84700	161000	154600	168300	190100	142800	146000	185100	139600	166700	164500	187900
$Fe_2O_3^{(T)}$	77100	35500	40800	68200	58300	21800	73400	68000	69900	78500	60400	61200	80400	59700	75600	75000	79200
MnO	1080	970	860	760	1010	1120	930	890	1000	930	930	850	950	1090	940	700	700
MgO	27200	14100	15900	24700	21100	8200	28400	25400	27700	31500	24600	28000	41800	27600	31100	29300	26500
CaO	22300	56100	45000	13100	50900	96800	27800	53100	41000	19100	77800	55400	21500	43700	26100	38500	25100
Na_2O	12400	25200	22800	16300	14400	24100	14700	12300	13100	13700	12800	14200	13700	15000	13400	9700	10200
K_2O	37700	17900	18600	32900	30800	11200	38100	34400	37200	41800	30800	33900	45800	30200	37000	38400	43200
TiO_2	8520	6590	6970	9410	7730	4550	8380	7880	8310	8210	7070	7540	8220	7380	8800	8810	8680
P_2O_5	1600	1100	1300	1700	1200	900	1500	1200	1400	1400	1100	1300	1800	1300	1800	1200	1300
LOI	65600	55500	58700	55300	74300	101200	75000	120300	92600	82800	148100	102600	81800	87100	75400	107800	82200
Sc	17	10	10	16	13	6	17	16	18	19	15	15	22	14	18	18	19
Be	3	1	1	3	2	1	3	3	3	4	2	2	4	2	3	3	3
V	110	73	77	121	85	48	122	117	129	144	106	133	155	105	137	163	143
Ba	429	553	573	384	440	213	425	504	518	518	431	453	533	563	548	468	455
Sr	103	216	215	91	267	609	118	252	321	199	321	276	190	640	275	173	189
Y	28	26	25	30	29	22	31	28	29	40	25	28	31	27	35	28	27
Zr	175	261	333	238	286	181	188	174	198	309	164	217	139	192	218	145	144
Cr	80	40	50	100	70	30	80	80	90	90	70	80	100	70	100	110	110
Co	22	9	9	17	14	4	19	17	19	22	15	16	25	21	20	20	21
Zn	150	60	60	120	90	27	110	100	120	130	100	100	140	760	120	130	110
Ga	22	12	12	20	16	8	21	20	21	27	17	18	26	17	21	23	24
Ge	3	2	2	3	2	2	3	3	3	3	2	2	3	2	3	3	3
Rb	155	61	63	130	111	38	144	129	143	161	110	123	175	112	142	158	164
Nb	14	10	9	15	12	6	14	13	17	42	11	12	13	12	21	14	14
Sn	4	2	2	4	3	1	4	3	4	6	3	3	4	5	4	4	4
Cs	8.9	2.3	2.8	7.6	5.9	1.5	8.7	8.2	9.2	10.1	7.2	7.4	11.3	6.5	8.9	9.1	9.5
La	37.3	24.2	26.2	34.4	37.1	19.7	37.4	36.7	38.3	38.6	28.7	31.8	34.4	26.6	40.2	35.5	40.8
Ce	79.4	51.4	53.1	72.4	77.4	45.8	79.6	83.9	82.6	89.2	62	67.4	80	59.3	84.8	74.6	83.9
Pr	8.92	6.32	6.27	8.06	8.35	5.46	8.6	9.02	9.07	9.04	6.78	7.17	8.91	6.7	9.23	8.24	9.16
Nd	34.2	24.7	24.7	31.1	31.7	23.1	33.8	35.1	35.8	36	26.5	27	36.5	27.7	35.5	31.3	34.6
Sm	7	5.3	4.9	6.3	6.4	4.6	7	6.3	6.9	8.2	5.1	5.6	7.2	5.7	7	6.4	6.8
Eu	1.5	1.12	1.02	1.37	1.28	1.13	1.36	1.38	1.37	1.57	1.12	1.21	1.59	1.25	1.47	1.32	1.39
Gd	6.1	4.7	4.5	5.9	5.6	4.2	6.1	5.9	5.9	7.7	4.8	5	6.3	5.2	6.8	5.7	5.9
Tb	1	0.8	0.7	1	0.9	0.6	1	0.9	0.9	1.3	0.8	0.9	1	0.8	1.1	0.9	0.9
Dy	5.6	4.7	4.3	5.6	5.4	3.7	5.5	5.4	5.7	7.4	4.4	5	5.7	4.6	6.6	5.1	5.6
Ho	1.1	0.9	0.9	1.2	1.1	0.7	1.1	1.1	1.1	1.5	0.9	1	1.1	0.9	1.3	1.1	1.1
Er	3.2	2.7	2.5	3.2	3.1	2	3.1	3	3.1	4.1	2.6	2.8	3.3	2.5	3.6	3.1	3.1
Tm	0.49	0.4	0.38	0.52	0.46	0.3	0.49	0.46	0.48	0.59	0.39	0.43	0.5	0.4	0.54	0.46	0.47
Yb	3.3	2.7	2.6	3.5	3.1	2.1	3.2	3	3.2	3.7	2.6	2.9	3.2	2.6	3.7	2.9	3.2
Lu	0.53	0.42	0.41	0.56	0.49	0.33	0.49	0.46	0.52	0.58	0.41	0.45	0.5	0.4	0.56	0.45	0.48
Hf	4.2	5.7	6.6	5.5	6.6	3.9	4.4	4.1	4.4	6.8	3.8	4.6	3.5	4.3	5	3.4	3.6
Ta	0.9	0.8	0.7	1.1	1	0.5	0.9	1.1	1.2	2.8	0.9	0.8	1.1	1	1.5	1	1
Tl	0.8	0.3	0.3	0.7	0.6	0.2	0.7	0.7	0.7	0.8	0.5	0.6	0.9	0.6	0.7	0.7	0.8
Pb	45	15	19	33	23	11	31	25	22	23	19	16	33	265	33	25	21
Th	11.6	7.8	7.8	11.4	9.7	5.6	11	10.3	11.2	14.1	8.8	9.8	12.4	9.3	11.5	12	12.2
U	2.8	2.1	2.1	3.1	2.8	1.7	3.2	3.2	3.5	4.8	2.8	3.6	4.5	3.3	3.3	3.5	3.1

Appendix A. Continued.

Core/	core	core	core	core	core	core	core	core	core	core	core	core	core	core	core	core	core
Surface	05-04	05-04	05-04	05-04	05-04	05-04	05-04	05-04	05-04	05-04	05-04	05-04	05-04	05-04	05-04	05-04	05-04
Lithology	ss	ss	ss	ss	ss	ss	ss	ss	st	ss	ss	ss	ss	st	ss	ss	ss
depth	511	515	520	526	540	548	562	568	576	596	597	609	628	665	680	682	688
unit	upper	upper	upper	upper	upper	upper	lower	lower	lower	lower	lower	lower	lower	lower	lower	lower	lower
SiO_2	716900	697600	680900	733200	714000	740300	712500	693700	679900	698800	713100	706400	674400	556200	631500	533300	664500
Al_2O_3	87100	106900	98400	89200	86500	85900	84200	105200	90500	105900	100200	96600	117900	167900	98800	178600	114700
$Fe_2O_3^{(T)}$	35500	39200	49500	34300	30300	34200	29300	43400	35800	45100	36300	38100	49600	81100	40500	81100	48900
MnO	830	640	690	640	710	710	830	650	920	560	730	860	820	700	1170	710	1140
MgO	11100	15000	14400	10800	10800	11700	10600	14100	11200	15800	14100	12400	16400	28800	14000	30100	18300
CaO	45800	34300	39500	34800	46800	36900	56800	29700	56700	23800	41700	43400	34300	32000	71900	34400	48800
Na_2O	17900	13900	14000	16700	16700	15400	15600	15000	14100	14900	16400	15800	14600	10700	13100	10300	13800
K_2O	17500	22600	21700	19600	17300	16100	16600	22500	19800	20900	17400	17500	24500	39300	18900	40900	22900
TiO_2	4640	6800	6930	4910	4560	6850	5050	7210	5470	7550	5590	5610	6800	9070	6370	9110	6850
P_2O_5	800	1400	1100	800	1000	1200	700	1400	800	1200	1000	1000	1100	1500	1200	1500	1400
LOI	54200	55200	56500	45500	53500	48500	64600	46000	77500	48900	55000	62000	62500	78800	91200	81800	68400
Sc	7	10	10	7	7	8	7	10	8	11	9	8	11	19	9	19	12
Be	1	2	2	1	1	1	1	2	1	2	2	1	2	3	2	3	2
V	52	74	71	50	50	64	54	76	58	82	66	64	82	138	67	137	85
Ba	350	276	275	809	325	269	360	290	509	265	250	282	360	435	546	470	558
Sr	87	86	84	203	179	115	269	97	275	90	113	217	130	178	503	191	221
Y	21	24	28	20	18	26	21	26	22	26	20	20	24	30	24	30	25
Zr	229	269	348	267	217	480	247	306	268	337	231	257	251	171	347	158	249
Cr	60	70	70	60	50	80	60	70	50	70	60	60	70	110	70	110	70
Co	7	12	12	8	6	8	7	11	9	11	10	9	12	20	11	20	13
Zn	40	280	290	180	60	60	40	80	60	100	70	90	80	110	130	110	80
Ga	10	13	13	10	10	10	9	13	10	14	12	11	15	22	11	22	14
Ge	2	2	2	2	2	2	2	2	2	2	2	2	2	3	2	3	2
Rb	64	86	81	72	64	62	58	85	70	81	68	66	87	148	66	150	85
Nb	7	10	11	8	7	10	8	11	8	11	8	8	10	13	9	14	11
Sn	2	3	3	2	2	2	2	3	2	3	2	2	3	4	2	4	3
Cs	2.5	4.2	3.7	2.7	2.6	2.5	2.4	4.2	3.3	4.1	3.3	3	4.5	8.1	3.4	8.8	4.6
La	22.7	26.1	30.3	21.7	21.4	31.6	22.1	31.5	24.6	33.6	25.3	24.2	31.4	39.3	26.1	38.4	29.3
Ce	47.7	58	65	45.5	46.3	66.5	48.6	67.6	53.8	69.7	53.3	52.1	65.1	83.5	58	81	64.9
Pr	5.65	6.84	7.48	5.34	5.14	7.64	5.63	7.19	6.12	7.73	6.06	5.9	7.44	9.07	6.5	8.92	6.79
Nd	21.9	27.6	30	21.2	21	29.4	22.2	30	25.8	29.1	23.8	22.8	27.6	36.1	26	34.9	27.7
Sm	4.6	5.8	5.8	4.6	4.1	6.2	4.8	5.8	5.3	5.3	4.6	4.8	5.2	6.5	5.5	6.8	5.7
Eu	0.95	1.15	1.17	0.91	0.89	1.18	0.96	1.23	1.13	1.06	0.93	0.99	1.14	1.4	1.04	1.33	1.18
Gd	4.3	5.2	5	3.9	3.9	5.3	4.1	5.6	4.8	4.4	4.3	4.2	4.6	5.6	5	5.6	5.1
Tb	0.7	0.8	0.9	0.6	0.6	0.9	0.7	0.8	0.7	0.7	0.7	0.7	0.8	0.9	0.8	0.9	0.8
Dy	4.1	4.5	4.9	3.6	3.4	5.1	3.9	5	4.2	4.5	3.9	3.9	4.3	5.4	4.3	5.2	4.8
Ho	0.8	0.9	1	0.7	0.6	1	0.8	1	0.8	0.9	0.8	0.8	0.9	1.1	0.9	1.1	0.9
Er	2.2	2.5	2.7	2	1.9	2.9	2	2.8	2.3	2.7	2.3	2.2	2.5	2.9	2.5	3	2.6
Tm	0.34	0.41	0.41	0.3	0.29	0.47	0.3	0.44	0.35	0.43	0.35	0.33	0.38	0.46	0.39	0.47	0.41
Yb	2.2	2.7	2.7	2.1	2	3.2	2	3	2.3	2.9	2.4	2.2	2.6	3.1	2.6	3	2.8
Lu	0.34	0.42	0.46	0.33	0.31	0.49	0.33	0.47	0.37	0.45	0.38	0.37	0.42	0.47	0.43	0.46	0.44
Hf	4.8	6.2	7.3	5.8	4.9	10.4	5.4	7.1	5.9	7.1	5	5.4	5.4	3.9	7.5	3.5	5.7
Ta	0.9	0.9	0.8	0.5	0.8	1.1	0.7	1	0.7	0.9	0.7	0.7	1.1	0.9	0.8	1.1	1
Tl	0.3	0.4	0.4	0.3	0.5	0.3	0.3	0.5	0.4	0.4	0.3	0.3	0.4	0.8	0.3	0.7	0.5
Pb	8	103	96	62	9	12	9	20	16	25	13	26	21	25	48	20	17
Th	6.9	8.3	9.1	7.1	5.5	9.7	6.5	7.5	7.3	9.4	7.4	7	8.8	11.4	8	11.9	7.5
U	1.7	2.4	2.2	1.7	1.5	2.6	1.8	2.4	2.1	2.8	2.1	2	2.6	3.2	2.4	3.1	2.3

Appendix A. Continued.

Core/	core	core	core	core	core	core	core	core	core	core	core	core	core	core	core	core	core
Surface	05-04	05-04	05-04	05-04	05-04	05-04	02-05	02-05	02-05	02-05	02-05	02-05	02-05	02-05	02-05	02-05	02-05
Lithology	ss	st	st	st	st	st	ss	cg	ss	ss	ss	ss	ss	ss	ss	ss	ss
depth	691	716	736	759	763	769	255	265	275	285	295	305	315	325	335	345	355
unit	lower	lower	lower	lower	lower	lower	upper	upper	upper	upper	upper	upper	upper	upper	upper	upper	upper
SiO_2	678400	572800	539300	527000	479000	537200	675800	726800	505300	536500	733200	686500	649000	720400	719100	680900	718200
Al_2O_3	93600	147800	174000	173000	185000	179400	112500	124400	87700	77400	115300	138000	118900	112400	110300	128600	121600
$Fe_2O_3^{(T)}$	32200	67300	77000	85100	92300	77900	41000	27600	34100	25000	47200	53500	47400	46900	41700	54100	51400
MnO	1410	850	740	800	810	710	780	530	730	880	630	750	850	480	620	730	460
MgO	14400	26200	29200	34800	47100	34100	16400	16700	13900	11500	18400	21700	17300	19000	15600	18900	18700
CaO	59700	48600	30200	32900	32100	29200	48800	14500	170700	170400	7800	11200	58200	4400	16000	26200	6400
Na_2O	14500	10700	9700	10300	7700	9700	21500	27700	10200	17400	18600	27500	26300	15000	21100	26000	22500
K_2O	18400	34300	42100	41300	44100	43400	23400	24100	22100	14000	23600	25000	22200	26700	24600	26000	25900
TiO_2	6680	8190	8530	8900	8230	8280	7480	8030	6260	6090	9280	8220	7940	7970	7480	8240	7980
P_2O_5	1200	1100	1200	1300	1300	1300	1300	1300	900	1000	1500	1400	1200	1100	700	1400	1400
LOI	63000	85600	84300	84000	101600	83600	56100	27200	155500	145100	29600	26000	57800	29500	29700	36800	26600
Sc	9	16	18	19	21	19	11	12	8	8	12	13	12	11	10	14	12
Be	2	3	3	3	3	3	2	2	1	1	2	2	1	2	1	2	2
V	64	115	123	141	177	131	85	80	67	56	95	97	86	86	80	97	89
Ba	263	395	548	467	395	490	368	952	698	271	413	600	404	412	441	412	396
Sr	166	209	245	193	169	221	128	141	137	148	99	151	149	81	117	136	107
Y	28	28	29	30	24	30	24	25	34	29	31	24	27	26	25	26	23
Zr	391	204	172	166	124	173	314	299	264	283	370	241	326	303	336	249	294
Cr	80	90	100	110	140	90	50	40	40	40	60	30	40	50	40	40	60
Co	10	17	20	20	25	20	10	10	5	2	12	11	8	13	8	11	13
Zn	50	100	100	100	280	100	60	50	40	40	60	60	50	80	50	60	80
Ga	11	19	22	22	24	22	11	12	9	7	12	12	11	14	10	11	16
Ge	2	3	3	3	3	3	1	1	1	1	2	1	1	2	1	1	2
Rb	66	125	157	155	163	155	70	69	65	40	71	72	61	92	68	72	88
Nb	10	13	14	14	12	14	13	12	12	11	16	10	12	14	13	11	14
Sn	2	3	4	4	5	4	2	2	2	2	3	2	2	2	2	2	2
Cs	3.4	7.3	9.1	9.1	9.4	9.1	3.4	2.8	4.1	2	3.9	3.6	2.9	4.1	3.1	3.8	3.9
La	27.8	32	38.9	43.6	35.6	38.1	28.7	30.1	35.8	23.1	37.1	35.1	30.6	39.3	25.9	36.8	36.2
Ce	62.5	67.5	83.7	91.7	74.5	81.4	56.3	62.6	58.1	47.3	78	73.7	59.3	71.2	62.8	63.3	60.1
Pr	7.32	7.58	9.27	9.76	8.12	8.86	6.31	7.35	8.71	6.13	8.47	7.82	6.9	7.12	7.03	7.05	6.63
Nd	29	29.4	36.4	35.9	29.6	33.9	23.2	28.1	33.8	23.8	31.8	28.2	25.6	26.1	28.4	25.4	22.4
Sm	6.3	6.1	6.6	6.6	5.8	6.9	4.5	5.4	6.7	4.8	6.3	5.1	5.1	5.2	5.8	5.2	4.5
Eu	1.27	1.27	1.33	1.32	1.21	1.33	0.96	1.09	1.38	0.99	1.26	1.06	1.14	1.05	1.17	1.17	0.99
Gd	5.9	5.4	5.8	5.6	4.8	5.8	4.1	4.4	6	4.2	5.4	4.1	4.4	4.6	4.8	4.5	4.1
Tb	0.9	0.9	0.9	0.9	0.8	0.9	0.7	0.7	0.9	0.7	0.9	0.7	0.7	0.8	0.7	0.8	0.7
Dy	4.9	5	5.3	5.6	4.6	5.4	4.1	4.1	5.5	4.2	5.3	4	4.4	4.9	4.2	4.5	4.4
Ho	1	1	1.1	1.1	0.9	1.1	0.8	0.8	1.1	0.9	1.1	0.8	0.9	1	0.9	0.9	0.9
Er	2.8	2.9	2.9	3.1	2.5	2.9	2.6	2.5	3.1	2.5	3.1	2.4	2.6	3	2.5	2.6	2.6
Tm	0.42	0.44	0.44	0.45	0.39	0.48	0.4	0.39	0.46	0.4	0.48	0.38	0.4	0.46	0.39	0.4	0.42
Yb	2.9	2.9	2.9	3.2	2.7	3.2	2.7	2.7	3.2	2.6	3.3	2.6	2.8	3.1	2.7	2.7	2.9
Lu	0.46	0.43	0.46	0.51	0.42	0.49	0.47	0.47	0.55	0.45	0.56	0.46	0.47	0.53	0.46	0.45	0.5
Hf	8.3	4.5	3.8	3.9	3	4.2	8.9	8.6	7.6	8.3	10.7	6.8	9.3	8.1	9.5	7.1	8.7
Ta	0.8	1.1	1	1	0.9	1	0.8	0.8	0.8	0.7	1.1	0.8	0.7	0.9	0.8	0.8	1
Tl	0.3	0.6	0.7	0.7	0.7	0.7	0.3	0.3	0.3	0.2	0.4	0.3	0.3	0.4	0.3	0.3	0.4
Pb	11	26	25	25	66	22	34	9	18	13	29	22	19	15	22	20	21
Th	8.8	10.2	11.4	12.2	11.2	11.9	9.1	9.3	7.6	7	9.8	9.3	9.2	8.1	8.6	9.3	9.7
U	2.7	2.9	3.1	3	3.6	3.4	2.7	2.2	2.5	2.3	3.1	2.7	2.5	2.5	2.6	2.9	2.6

Appendix A. Continued.

Core/	core	core	core	core	core	core	core	core	core	core	core	core	core	core	core	core	core
Surface	02-05	02-05	02-05	02-05	02-05	02-05	02-05	02-05	02-05	02-05	02-05	02-05	02-05	02-05	02-05	02-05	02-05
Lithology	cg	ss	ss	cg	ss	ss	ss	ss	ss	ss	ss	ss	cg	ss	cg	ss	ss
depth	365	375	385	395	405	415	425	435	445	455	465	475	485	495	505	515	525
unit	upper	upper	upper	upper	upper	upper	upper	upper	upper	upper	upper	upper	upper	upper	upper	upper	upper
SiO_2	646000	746300	742100	678200	590600	706100	641700	522100	600700	696300	668700	336600	690900	680900	638700	647900	689300
Al_2O_3	119000	112000	113000	135700	113800	117800	94900	164300	163900	127600	115800	69000	117800	107500	145600	103800	104700
$Fe_2O_3^{(T)}$	36100	44400	42800	55800	46600	44200	45000	56400	82100	42700	39500	36300	47400	40000	71600	40400	38000
MnO	1130	440	600	630	1900	670	690	830	900	740	950	1270	720	1040	690	770	1130
MgO	14700	17000	15500	25400	15400	17000	14600	33500	32700	16600	16100	12700	18100	16300	24300	16900	13400
CaO	66700	7500	14700	13900	98400	16000	82000	61700	5800	26500	52000	278900	31100	52100	9500	64900	51500
Na_2O	28800	21500	26400	15000	26900	19800	16600	5600	10700	32200	27500	7500	21400	23800	17500	16300	26600
K_2O	23900	26000	23500	30900	20100	28100	21900	47700	40400	22800	22300	18600	26500	23100	34400	25100	20800
TiO_2	5740	7450	7210	8880	7640	7980	6590	7770	9110	6510	6470	4460	8270	6020	9800	7490	6320
P_2O_5	1200	1300	1400	1400	1500	600	1200	1100	1400	1400	1500	1100	1400	1200	1300	1000	1400
LOI	61800	23600	18400	42000	77900	30700	78400	98100	47800	28400	49300	235200	44800	56500	44600	72000	47500
Sc	10	11	10	13	12	12	9	17	17	11	10	7	12	10	15	10	9
Be	1	2	1	2	1	2	1	4	4	1	1	1	2	2	3	2	1
V	67	83	74	88	85	85	64	119	124	80	72	56	92	69	119	84	65
Ba	561	466	418	407	387	453	326	433	468	454	417	210	372	362	418	568	379
Sr	150	104	143	90	208	106	110	87	89	165	159	182	113	121	84	104	150
Y	22	23	24	30	31	24	26	29	33	21	24	23	30	24	32	30	24
Zr	188	317	324	308	225	344	266	171	273	196	227	160	434	251	292	321	225
Cr	20	40	40	70	40	100	50	90	90	30	40	40	50	40	90	60	40
Co	7	10	9	17	6	11	8	19	21	9	9	0.9	10	8	18	11	7
Zn	60	60	70	120	60	80	60	150	130	60	60	50	80	80	130	100	60
Ga	12	12	13	19	13	15	11	24	24	14	13	9	13	12	22	14	11
Ge	1	2	2	2	1	2	2	2	3	1	2	1	2	2	2	2	2
Rb	69	74	73	112	61	96	69	171	152	72	68	62	82	72	133	104	65
Nb	11	13	11	18	11	14	13	17	27	10	10	9	16	10	20	15	9
Sn	1	2	1	2	1	2	1	3	4	1	1	0.9	3	1	3	2	1
Cs	2.6	3.4	2.6	6.1	2.1	4.4	2.9	11	9.6	2.7	2.4	3.7	4.4	3	7.9	5.1	2.5
La	35.7	34.3	29.6	43.6	32.9	24.9	30.2	40.9	43.2	29.7	31.2	22	39.5	26.6	43.9	33.4	28.9
Ce	62	55.8	58.6	68.4	74.8	48.2	48.9	61.6	81.3	56.3	53.4	45.7	67.9	46.5	73.4	42.9	54.5
Pr	7.24	5.98	6.58	7.4	8.71	5.45	6.17	6.92	8.62	6.4	6.3	5.73	7.35	5.46	7.94	5.94	6.35
Nd	25.9	21.4	23.5	25.4	31.1	19.3	21.6	23	29	23.1	21.9	20.5	26.6	19.7	27.6	21	22.3
Sm	4.7	4.2	4.8	5.5	6.2	4	4.6	4.8	6.5	4.7	4.5	4.3	5.4	4.1	6	4.6	4.6
Eu	0.99	0.91	1.06	1.17	1.41	0.88	0.98	1.05	1.3	1.07	1.03	0.94	1.03	0.9	1.27	0.97	1.03
Gd	3.8	3.9	4.2	5	5.3	3.7	4.1	4.4	5.7	3.8	3.8	4	5	3.6	5.3	4.3	4.1
Tb	0.6	0.7	0.7	0.9	0.8	0.7	0.7	0.8	1	0.6	0.7	0.7	0.9	0.6	0.9	0.8	0.7
Dy	3.7	4.1	4.1	5.4	4.9	4.3	4.4	5.2	6.3	3.7	3.9	3.9	5.2	3.8	5.8	5	4
Ho	0.7	0.8	0.8	1.1	1	0.9	0.9	1.1	1.3	0.7	0.8	0.8	1.1	0.8	1.2	1	0.8
Er	2.2	2.5	2.4	3.2	2.8	2.7	2.6	3.1	3.6	2.1	2.3	2.1	3.1	2.3	3.5	3	2.3
Tm	0.33	0.39	0.38	0.5	0.41	0.42	0.41	0.48	0.56	0.33	0.35	0.31	0.47	0.35	0.53	0.48	0.35
Yb	2.4	2.7	2.6	3.4	2.8	2.9	2.8	3.3	3.8	2.2	2.4	2.1	3.3	2.4	3.6	3.3	2.4
Lu	0.41	0.45	0.44	0.57	0.45	0.51	0.46	0.55	0.64	0.36	0.41	0.32	0.55	0.39	0.6	0.57	0.4
Hf	5.5	8.5	9.2	9.3	6.5	10.2	7.8	5.4	8.1	5.7	6.6	4.6	12	7	8.9	9.5	6.5
Ta	0.6	0.8	0.8	1.2	0.7	1	0.8	1.1	1.8	0.7	0.7	0.6	1.1	0.7	1.4	1	0.7
Tl	0.3	0.4	0.3	0.5	0.3	0.4	0.3	0.9	0.8	0.3	0.3	0.3	0.4	0.3	0.7	0.5	0.3
Pb	13	20	18	20	15	15	17	15	43	16	13	26	27	16	34	20	16
Th	7.1	8.7	8.4	11.2	7.8	9.8	7.3	11.2	12.7	10.5	8.2	5.5	10.6	7.4	12.1	9.1	7.5
U	2	2.7	2.2	3.2	2	2.9	2.3	3.9	3.4	2.2	2	2.2	3.4	1.9	3.4	3.3	1.9

Appendix A. Continued.

Core/	core	core	core	core	core	core	core	core	core	core	core	core	core	core	core	core	core
Surface	02-05	02-05	02-05	02-05	02-05	02-05	02-05	02-05	02-05	02-05	02-05	02-05	02-05	02-05	02-05	02-05	02-05
Lithology	cg	ss	ss	ss	ss	cg	ss	ss	st	st	st	ss	ss	ss	ss	ss	ss
depth	535	545	555	565	575	585	595	605	615	625	635	645	655	665	675	685	695
unit	upper	upper	upper	upper	upper	upper	upper	upper	upper	upper	upper	upper	upper	upper	upper	upper	lower
SiO_2	706900	704000	604000	690800	676000	678200	741700	684500	317600	511700	499500	321600	544400	724400	550800	732700	568700
Al_2O_3	115900	123700	125400	118400	103600	128700	93900	120800	77100	135600	93000	104800	93300	110300	208800	81400	145700
$Fe_2O_3^{(T)}$	42000	49100	32300	47400	47700	49200	34700	44400	33800	55400	25100	44300	35300	48000	66200	33500	66200
MnO	770	640	1000	990	1450	780	1050	770	560	720	760	410	890	580	480	960	560
MgO	15100	18300	18600	17900	14200	17100	12300	17800	12400	23900	12600	16200	12800	14900	30700	10500	20000
CaO	29600	18400	86200	28500	51300	22800	36400	33300	193700	76800	124300	186400	115900	24000	7900	47000	54000
Na_2O	29700	31200	29000	20800	27600	26700	21500	21700	8300	15800	13300	6100	13500	14000	9500	15700	11500
K_2O	22500	23200	23900	24700	16600	26400	16100	25300	18900	29600	20800	26900	21400	24100	52100	16300	35800
TiO_2	6580	8110	7570	7910	9950	7640	7390	7610	4090	6540	5980	5050	5070	7260	9770	5060	7970
P_2O_5	1400	1600	1000	1300	1900	1600	2000	1500	900	1800	1400	1100	1100	1600	1900	1200	1300
LOI	34100	28000	78300	45100	48100	38200	39700	47000	138400	83400	104400	90900	96500	41000	60600	53700	71700
Sc	10	13	13	11	12	12	9	11	8	13	9	11	9	10	21	7	16
Be	1	2	2	2	1	2	1	2	1	2	1	2	2	2	4	1	3
V	75	91	101	73	81	92	68	90	64	101	127	87	64	75	161	49	112
Ba	909	689	391	344	288	406	244	344	363	451	662	342	539	272	462	320	736
Sr	200	184	190	108	164	139	253	288	935	771	2751	1542	1205	85	93	311	664
Y	23	26	25	27	37	25	33	29	15	24	20	19	19	24	30	22	28
Zr	270	336	278	282	633	309	397	329	108	194	241	89	207	349	165	260	206
Cr	40	50	50	60	60	60	70	70	30	50	40	70	40	80	130	60	90
Co	9	11	11	13	8	11	9	13	5	15	8	8	7	12	28	7	17
Zn	60	70	70	80	60	80	60	80	70	160	70	80	90	70	120	50	90
Ga	13	14	15	15	12	15	11	14	10	15	10	14	11	14	28	10	19
Ge	2	2	2	2	2	2	2	2	0.9	1	1	1	1	2	2	2	2
Rb	72	79	85	87	54	86	53	88	63	89	66	96	70	86	184	55	124
Nb	12	13	12	13	14	14	13	14	9	11	10	9	13	16	19	10	15
Sn	1	2	1	2	1	2	1	2	1	3	2	1	2	2	4	1	3
Cs	2.8	3.4	3.6	4.7	2.4	4.1	2.4	4.5	3.9	6.3	4.1	6.1	3.9	4.6	10.6	2.5	7.3
La	32	38.3	23.5	34.3	38.3	32	31.6	27.4	29.2	31.8	25.6	25.5	28.5	33.4	51.4	23.9	41.7
Ce	55.7	72.4	48.5	58.4	77.8	61.4	66.1	57.4	51.9	62.5	49.5	49	53.3	64.1	97.1	48.2	80.6
Pr	6.36	8.41	5.96	6.49	8.86	6.91	8.11	7.18	5.4	6.96	5.62	5.64	6.2	7.33	10.7	5.93	9.02
Nd	22.2	30.2	21.2	22	31.4	24.4	30.6	26.5	18.2	26.3	21.3	20	23.4	25.6	35.2	22.5	31
Sm	4.6	5.9	4.4	4.7	6.4	5.1	6.8	5.7	3.4	5.4	4.4	3.9	5	5.2	6.5	5	5.6
Eu	1.02	1.21	1.06	1.04	1.38	1.08	1.35	1.17	0.67	1.13	0.86	0.84	1	1	1.34	1	1.14
Gd	4.1	5.1	3.9	4.3	5.8	4.4	5.9	4.9	2.7	4.7	3.9	3.4	3.9	4.3	5.4	4.4	4.7
Tb	0.7	0.8	0.7	0.8	1	0.7	1	0.8	0.4	0.8	0.6	0.6	0.6	0.7	0.9	0.7	0.8
Dy	4.1	4.8	4.1	4.8	6	4.5	5.6	4.8	2.6	4.5	3.7	3.4	3.6	4.3	5.3	4	4.8
Ho	0.8	1	0.8	1	1.2	0.9	1.1	1	0.5	0.9	0.7	0.7	0.7	0.9	1.1	0.8	1
Er	2.4	2.8	2.5	2.8	3.6	2.7	3.1	2.8	1.5	2.5	2.2	1.9	2	2.5	3.2	2.2	2.8
Tm	0.38	0.44	0.39	0.44	0.56	0.42	0.47	0.43	0.23	0.4	0.33	0.29	0.31	0.39	0.49	0.33	0.43
Yb	2.5	3	2.7	3.1	4	2.9	3.2	3	1.5	2.7	2.2	1.9	2.1	2.7	3.3	2.3	2.9
Lu	0.42	0.5	0.45	0.52	0.7	0.48	0.55	0.5	0.26	0.45	0.36	0.32	0.35	0.45	0.53	0.37	0.49
Hf	8	9.7	8.1	8.2	17.7	8.9	11.2	9.3	3	5.2	6.6	2.7	5.7	9.9	5	7.3	6.2
Ta	0.8	0.9	0.8	1	1	1	0.9	0.9	0.5	0.8	0.7	0.7	0.7	1	1.3	0.7	1
Tl	0.3	0.4	0.4	0.4	0.2	0.4	0.3	0.4	0.3	0.5	0.3	0.4	0.3	0.4	1	0.3	0.6
Pb	20	22	18	29	24	25	20	26	13	30	20	9	49	13	21	9	20
Th	8.8	10.2	9.7	9.4	12.8	10.4	9.3	9.4	4.8	8.3	7.7	6.8	6.4	9.2	13.5	7	10.4
U	2.3	2.6	2.8	2.7	3.2	2.7	2.6	2.9	1.5	2.5	2.7	1.9	1.7	2.6	3.8	2	2.8

Appendix A. Continued.

Core/	core	core	core	core	core	core	core	core	core	core	core	core	core	core
Surface	02-05	02-05	02-05	02-05	02-05	02-05	02-05	02-05	02-05	02-05	02-05	02-05	02-05	02-05
Lithology	ss	ss	ss	st	st	st	ss	ss	ss	ss	st	ss	st	ss
depth	705	715	725	735	745	755	765	775	785	795	805	815	825	835
unit	lower	lower	lower	lower	lower	lower	lower	lower	lower	lower	lower	lower	lower	lower
SiO_2	711200	668900	681500	549600	537000	650100	566900	628600	554400	559900	578100	283900	658300	533700
Al_2O_3	88200	119500	107600	176700	196900	104000	168800	101900	184100	166200	154300	74600	108100	163200
$Fe_2O_3^{(T)}$	32400	50100	42800	79300	89900	34500	77100	34500	86100	71600	64700	30900	42100	62800
MnO	1240	870	1130	590	610	1730	730	1670	650	790	800	320	1510	1020
MgO	11200	16200	14900	28100	28700	15500	27600	17500	31800	32000	33300	17700	21400	48400
CaO	59900	37900	48500	23800	15300	76600	29400	85300	15800	37100	42100	223900	59600	42500
Na_2O	16300	13300	14300	9600	9000	13400	10100	12500	9400	10500	10800	5700	13600	9000
K_2O	16500	26900	22700	45400	50400	21100	42000	21000	44400	39400	36100	16800	21800	38200
TiO_2	4780	7340	6460	8200	8530	6750	8390	6120	8920	8560	7840	3910	6990	8050
P_2O_5	1100	1300	1300	1600	1700	1300	1500	1200	1400	1600	1400	800	1400	1500
LOI	61800	55400	60100	68300	64800	82400	68400	92000	62500	75100	76100	81600	71900	91200
Sc	7	11	10	19	21	9	17	9	19	17	15	7	10	18
Be	1	2	2	3	4	2	3	2	3	3	3	1	2	3
V	54	84	66	146	156	69	142	73	147	130	117	48	77	138
Ba	358	335	654	460	477	307	497	666	460	408	581	214	360	440
Sr	267	108	223	123	133	124	152	432	117	134	359	701	201	166
Y	24	28	25	29	28	28	28	28	27	29	29	15	30	30
Zr	223	309	273	146	155	282	168	384	176	179	200	92	269	198
Cr	50	80	70	100	120	80	110	80	120	110	100	50	80	110
Co	9	14	13	21	24	11	21	11	23	20	18	4	11	23
Zn	50	80	70	110	120	70	110	70	120	120	110	70	70	200
Ga	10	15	13	22	27	13	23	13	25	22	19	10	14	22
Ge	2	2	2	2	3	2	2	2	2	2	2	1	2	2
Rb	56	93	78	149	176	75	148	75	164	142	127	62	80	138
Nb	10	14	13	16	17	14	17	12	20	18	16	9	15	16
Sn	1	2	2	4	4	2	3	2	4	3	3	1	2	4
Cs	2.8	5.2	4.2	9.8	10.6	4.2	9.2	4.4	10	8.6	7.5	3.8	4.7	8.8
La	23.8	37.7	31.5	44.1	50.5	30	46.8	31.1	48.7	43.8	35.6	18.8	33.6	39.6
Ce	48.7	76.2	63.4	84.1	100	62.1	90.8	63.6	93.1	85	70.1	36.3	71.5	79.3
Pr	6.1	8.66	7.33	9.3	11.1	7.53	10.2	7.46	10.4	9.71	8.1	4.23	8.49	8.99
Nd	23.3	30.2	26.3	34.4	37.2	28	33.9	27.6	34.9	34	28.6	14.6	31.4	31.9
Sm	5.5	6.1	5.7	6.2	6.6	6.1	6.4	6.3	6.4	6.8	5.9	3	6.7	6.5
Eu	1.16	1.21	1.19	1.29	1.33	1.27	1.29	1.19	1.33	1.38	1.22	0.6	1.24	1.32
Gd	4.8	5.2	4.9	5.4	5.3	5.5	5.2	5.3	5.4	5.7	5.2	2.5	5.8	5.4
Tb	0.8	0.9	0.8	0.9	0.9	0.9	0.9	0.9	0.9	1	0.9	0.4	0.9	0.9
Dy	4.4	5	4.6	5.2	5.3	5	5.2	4.9	5.5	5.6	5	2.5	5.5	5.2
Ho	0.8	1	0.9	1	1.1	1	1	1	1.1	1.1	1	0.5	1.1	1
Er	2.2	2.9	2.5	2.9	3.1	2.8	3	2.8	3.3	3.2	2.8	1.4	3.1	2.9
Tm	0.34	0.44	0.39	0.45	0.47	0.42	0.45	0.41	0.5	0.48	0.43	0.22	0.46	0.44
Yb	2.3	3	2.6	3	3.2	2.9	3	2.8	3.4	3.2	2.9	1.5	3.2	3
Lu	0.37	0.49	0.44	0.49	0.55	0.49	0.52	0.48	0.56	0.54	0.51	0.25	0.54	0.51
Hf	6.2	9	7.6	4.3	4.6	8.4	5.1	11	5.6	5.6	5.7	2.8	7.9	5.8
Ta	0.7	1	0.9	1	1.2	1	1.2	0.9	1.3	1.2	1.1	0.6	1	1.1
Tl	0.3	0.4	0.4	0.7	0.8	0.3	0.7	0.4	0.7	0.6	0.6	0.3	0.4	0.6
Pb	11	22	20	29	27	17	31	17	26	31	30	17	19	33
Th	6.7	9.6	8.3	11.3	12.7	8.6	11.7	9.3	13.3	11.9	10.4	5.3	9	11
U	1.9	2.9	2.4	3.3	3.5	2.6	4	2.7	3.6	3.4	3.1	1.6	2.7	3.4

Notes: data in ppm; ss = sandstone; st = siltstone or finer grained.